

Arsenic-Imposed Effects on Schwertmannite and Jarosite Formation in Acid Mine Drainage and Coupled Impacts on Arsenic Mobility

Edward D. Burton,* Niloofar Karimian, Scott G. Johnston, Valerie A. Schoepfer, Girish Choppala, and Dane Lamb



Cite This: *ACS Earth Space Chem.* 2021, 5, 1418–1435



Read Online

ACCESS |



Metrics & More



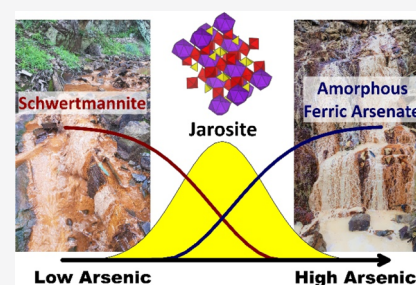
Article Recommendations



Supporting Information

ABSTRACT: This study explores interactions between As and Fe(III) minerals, predominantly schwertmannite and jarosite, in acid mine drainage (AMD) via observations at a former mine site combined with mineral formation and transformation experiments. Our objectives were to examine the effect of As on Fe(III) mineralogy in strongly acidic AMD while also considering associated controls on As mobility. AMD at the former mine site was strongly acidic (pH 2.4 to 2.8), with total aqueous Fe and As decreasing down the flow-path from ~ 400 to ~ 20 mg L⁻¹ and $\sim 33,000$ to ~ 150 μ g L⁻¹, respectively. This trend was interrupted by a sharp rise in aqueous As(III) and Fe(II) caused by reductive dissolution of As-bearing Fe(III) phases in a sediment retention pond. Attenuation of Fe and As mobility occurred via formation of As(V)-rich schwertmannite, As(V)-rich jarosite, and amorphous ferric arsenate (AFA), resulting in solid-phase As concentrations spanning ~ 13 to ~ 208 g kg⁻¹. Schwertmannite and jarosite retained As(V) predominantly by structural incorporation involving AsO₄³⁻-for-SO₄²⁻ substitution at up to ~ 40 and ~ 22 mol %, respectively. Arsenic strongly influenced Fe(III) mineral formation, with high As(V) concentrations causing formation of AFA over schwertmannite. Arsenic also strongly influenced Fe(III) mineral evolution over time. In particular, increasing levels of As(V) incorporation within schwertmannite were shown, for the first time, to enhance the transformation of schwertmannite to jarosite. This significant discovery necessitates a re-evaluation of the prevailing paradigm that As(V) retards schwertmannite transformation.

KEYWORDS: AMD, arsenate, jarosite, mining, schwertmannite



INTRODUCTION

Acid mine drainage (AMD) is one of the most significant environmental issues faced by the mining industry worldwide.¹ AMD is formed by microbially mediated oxidation of sulfide minerals (e.g., pyrite and FeS₂) in the absence of sufficient acid-neutralizing capacity.² This occurs following exposure to oxygenated water in, for example, metal sulfide mines and associated mine wastes. The resulting waters are strongly acidic, enriched in Fe and SO₄²⁻, and often have elevated As concentrations resulting from oxidative weathering of arsenopyrite (FeAsS) or As-bearing pyrite (FeS₂).³ In most AMD systems, the mobility and fate of As are largely controlled by interactions with abundant Fe(III) minerals via adsorption and coprecipitation processes.^{4–6}

Microbially mediated oxidation of soluble Fe(II) in AMD into less soluble Fe(III) leads to oversaturation with respect to Fe(III) minerals. Initially, high levels of oversaturation kinetically favor the formation of poorly ordered Fe(III) phases, such as schwertmannite [Fe₈O₈(OH)₆SO₄].^{6–9} Poorly ordered hydrous Fe(III)–As(V) oxides or hydroxysulfates may also form from waters with high As(V)/Fe(III) ratios.^{9–12} Over time, crystalline Fe(III) minerals such as goethite (α -FeOOH), jarosite [KFe₃(SO₄)₂(OH)₆], and scorodite (FeAsO₄·2H₂O) may replace the initial poorly ordered

phases.^{8,13–16} These minerals can be important host phases for As under acidic-oxidizing conditions,¹⁷ yet may act as As sources under reducing conditions (e.g., as a result of burial in the presence of labile organic matter) and/or higher pH conditions (e.g., as a result of AMD neutralization).^{18–21}

Although many studies of AMD systems have been conducted, relatively few have examined As-imposed constraints on the formation and fate of As-hosting Fe(III) minerals, such as schwertmannite and jarosite, at sites having strongly acidic (pH < 3) and As-rich AMD.²² A robust understanding of the formation and behavior of As-hosting Fe(III) minerals at such sites is important to the development of accurate risk assessment models and the formulation of reliable remediation strategies. Site-specific geochemical and mineralogical information is particularly critical to accurate prediction of how As mobility may be controlled by and may itself influence long-term mineral transformations, such as the

Received: February 15, 2021

Revised: March 28, 2021

Accepted: April 25, 2021

Published: May 19, 2021



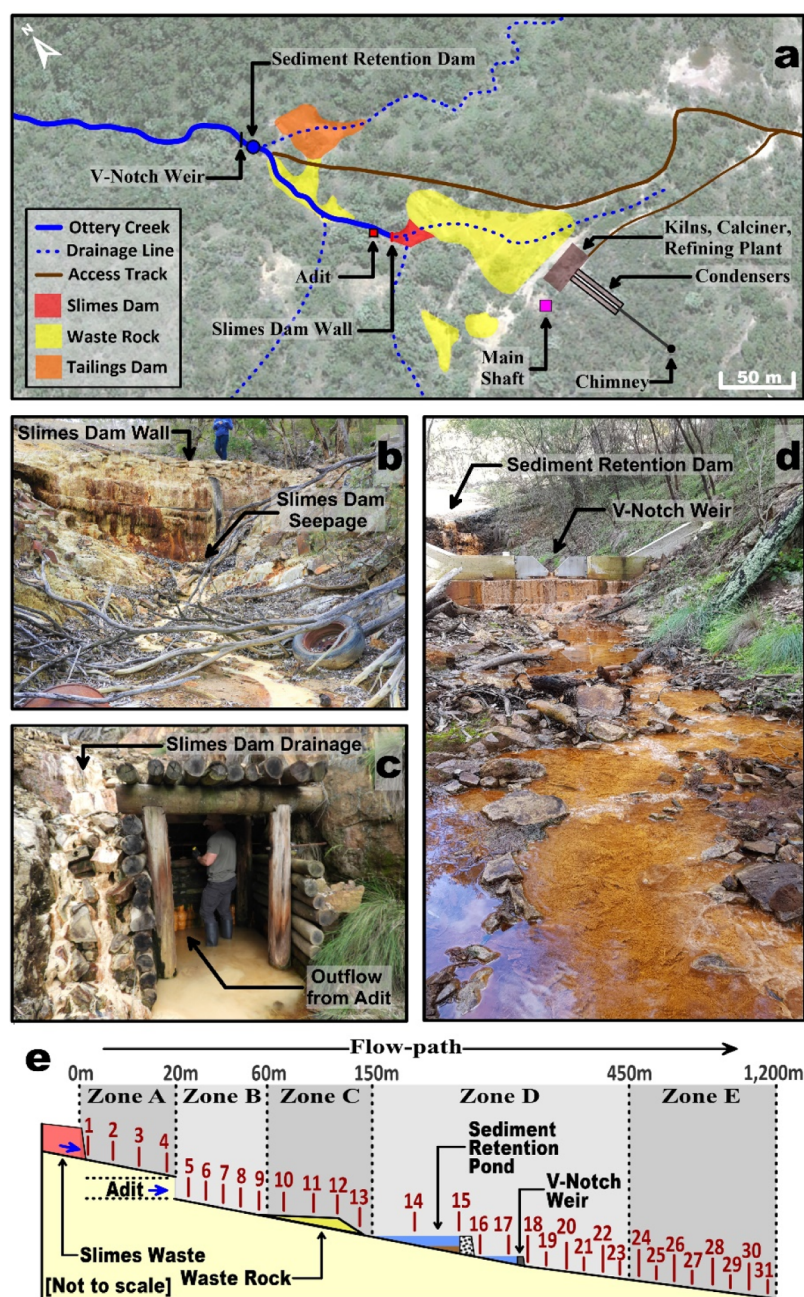


Figure 1. Map of the study site (a), with photographs of key locations along the AMD flow-path (presented as the solid-blue line and labeled as Ottery Creek) showing the slimes dam wall (b), mixing zone between discharge from the slimes dam and disused adit (c), area downstream of V-notch weir/sediment retention pond (d), and conceptual diagram showing the position of water sampling sites along the AMD flow-path (shown as red numbers) in relation to key site features and distinct geochemical and mineralogy zones (e).

transformation of schwertmannite to goethite and jarosite.^{13,14,16,23–27} Such information is also critical to understanding the potential shift between Fe(III) minerals acting to either immobilize or release As into surface water under existing site-specific conditions or future remediation scenarios.

In this study, we investigate interactions between As and Fe(III) minerals (predominantly schwertmannite and jarosite) in strongly acidic ($\text{pH} < 3$) and As-rich AMD via field-based observations at a former mine site combined with laboratory-based mineral formation and transformation experiments. We focus specifically on Fe(III) minerals which have precipitated from AMD (i.e., waters that are separated from their source in mining wastes and mine workings). Our objectives were to

examine the effect of As on Fe(III) mineralogy in strongly acidic AMD, while also considering associated controls on As mobility. The results provide new insights into As-imposed constraints on the formation and stability of Fe(III) minerals, particularly schwertmannite and jarosite, as well as the impact of these minerals on As mobility and fate in AMD systems.

■ MATERIALS AND METHODS

Field-Based Observations: Study Site and Sample Collection. Water samples and associated As- and Fe-rich ochreous precipitates were collected from an AMD system at a former As–Sn mine site in eastern Australia (Figure 1; see

Supporting Information for a detailed description of the study site).

Water samples were collected at multiple locations along the AMD flow-path (Figure 1) on three occasions in July, 2020. Sampling was conducted on three separate occasions in order to provide a degree of temporal replication in sampling (to account for short-term temporal variability). At each AMD surface-water sampling location, pH, redox potential (corrected to standard hydrogen electrode), and temperature were measured using HACH HQd portable meters and freshly calibrated probes. In addition to surface waters, sediment pore-water samples (from the surface 0–3 cm depth interval) were also collected from a sediment retention pond located along the AMD flow-path using a push-tube coring approach with subsequent centrifugation for separation of pore-water.²⁸ Surface- and pore-water samples were filtered to <0.45 μm using syringe-driven cellulose acetate filters and preserved via acidification with HNO_3 to $\text{pH} < 2$ for subsequent quantification of total element concentrations. A separate filtered aliquot was preserved via acidification with HCl (to 1% v/v) and stored in the dark at 4 $^\circ\text{C}$ for quantification of aqueous As speciation and aqueous Fe^{2+} .²⁹

Samples of ochreous Fe(III) -rich accumulations were collected from multiple locations along the AMD flow-path in parallel with the water sampling, as described above. The samples were frozen at -80 $^\circ\text{C}$ within 6 h after collection and were subsequently freeze-dried and sieved at <180 μm .

Laboratory-Based Experimentation: Mineral Formation and Transformation. The effect of As(V) on the formation and transformation of Fe(III) minerals produced by Fe(II) oxidation under acidic and SO_4 -rich conditions was examined in a series of laboratory-based experiments. These experiments were designed to mimic key aspects of the in situ conditions under which Fe(III) minerals form and transform in AMD systems. The experiments involved mixing, by vigorous magnetic stirring, a 3 L solution containing 0.04 M $\text{FeSO}_4 \cdot 7\text{H}_2\text{O}$ and 0.01 M K_2SO_4 with 1 L of a second solution containing 1.5% H_2O_2 and various concentrations of aqueous As(V) (prepared from $\text{Na}_2\text{HAsO}_4 \cdot 7\text{H}_2\text{O}$). The As(V) concentrations were selected to give final molar Fe/As ratios of 32, 16, 8, 4, and 2, in addition to an As -free treatment. These molar Fe/As ratios allow comparability with the range of in situ solid-phase molar Fe/As ratios in Fe(III) minerals formed from AMD at the study site. Potassium was included in these experiments, in contrast to earlier comparable mineral formation and transformation experiments,^{11,12,16,26,30–32} in order to create conditions that allow the formation of jarosite, which (as shown below) was a key Fe(III) mineral at the study site.

After mixing, the final solutions were allowed to stand for 4 h, during which a solid precipitate formed. The suspension pH was adjusted to 2.7 by dropwise addition of 6 M KOH and allowed to stand for a further 20 h (prior to repeated pH adjustment to 2.7). Samples of the suspension were then retrieved for analysis of aqueous- and solid-phase properties, as described below. Longer-term mineral transformations were examined by aging the suspensions at 60 $^\circ\text{C}$ (twice daily mixing by shaking) with samples collected and analyzed for aqueous- and solid-phase properties at aging times of 2, 5, and 10 days. In accordance with previous experiments into the effect of As(V) on schwertmannite transformation,¹⁶ a temperature of 60 $^\circ\text{C}$ was used in order to accelerate mineral transformation relative to the slower rates that occur at

ambient temperature. By conducting the mineral transformation experiment at 60 $^\circ\text{C}$, aging times of only 2–10 days were sufficient to allow significant formation of crystalline Fe(III) phases from precursor poorly ordered phases, thereby allowing comparison with the in situ mineralogy observed at the study site.

Analyses. Quantification of total As and a range of other elements (including Fe, K, and S) in water samples and selective extracts was achieved via inductively coupled plasma mass spectrometry (ICP–MS; PerkinElmer ELAN–DRCe) or ICP optical emission spectrometry (ICP–OES; PerkinElmer Avio 500). Arsenic speciation was determined, within 7 days of sampling, via high-performance liquid chromatography (HPLC; PerkinElmer Flexar) coupled with ICP–MS (PerkinElmer Nexion 350D), using a C18 (5 μm) column and mobile phase of 1 mM tetra-butyl ammonium hydroxide, 0.5 mM EDTA, and 5% ethanol in de-ionized water (flow rate 1 mL min^{-1} ; 20 μL injection).³³ The sum of aqueous As(III) and As(V) determined via HPLC–ICP–MS matched the total As results from ICP–MS within 15% for As concentrations >10 $\mu\text{g L}^{-1}$. Aqueous Fe(II) and total aqueous Fe concentrations were determined using the 1,10-phenanthroline method³⁴ within 12 h of sampling. Fe(III) was calculated as the difference between total aqueous Fe and Fe(II) . Total aqueous Fe concentrations determined by the 1,10-phenanthroline method matched the corresponding ICP–OES results within 10%. The quality of the results was assured by measuring standards and blanks during each analytical run (typically included at a frequency of every 10 samples), as well as triplicates on 10–20% of samples (with the relative standard deviation being <4% for As, Fe, S, and K).

Mineralogy was examined using X-ray diffraction (XRD) on randomly orientated powders with a Bruker D4 Endeavor fitted with a Co X-ray source and LYNXEYE detector (10–90 2θ with a 0.04 $^\circ$ 2θ step-size and a 4 s count-time). The resulting patterns were analyzed using the DIFFRAC-plus evaluation software package (Bruker AXS, Karlsruhe, Germany) and the PDF-4/Mineral database from the International Centre for Diffraction Data. In order to aid identification of poorly ordered phases, XRD patterns were also collected for 2-line ferrihydrite, schwertmannite, and amorphous ferric arsenate (AFA), which were synthesized using standard methods.^{35,36} Selected solid-phase samples were examined by scanning electron microscopy (SEM; Carl Zeiss EVOL 15) on carbon- and gold-coated samples mounted on aluminum stubs. The elemental composition at points of interest was determined by energy dispersive X-ray (EDX) analysis with an Oxford INCA X-Act SDD X-ray detector.

The total concentrations of As, Fe, and other elements were extracted from solid-phase samples by microwave-assisted aqua regia digestion in poly(tetrafluoroethylene) containers. The abundance of poorly crystalline versus crystalline Fe(III) phases, along with associated As and other elements, was determined using selective ammonium oxalate extractions.³⁷ Poorly crystalline Fe(III) phases were extracted by shaking 100 mg of the freeze-dried precipitate with 40 mL of 0.2 M ammonium oxalate (adjusted to pH 3.0) at room temperature for 2 h in the dark. The same ammonium oxalate extractant was used to also extract crystalline Fe(III) phases, along with poorly ordered phases, by shaking for 4 h at 80 $^\circ\text{C}$, respectively. Research by Drahota et al.³⁷ demonstrates that this oxalate extraction scheme is capable of accurately quantifying the abundance of poorly ordered Fe(III) phases

(which in this study comprise schwertmannite and AFA, as described below) versus their crystalline counterparts (which include jarosite, scorodite, and goethite). Surface-adsorbed As(III) and As(V) were extracted by shaking 200 mg with 40 mL of 0.01 M NaH_2PO_4 for 16 h at room temperature in the dark.³⁷ Extracted elements and the abundance of surface-adsorbed As(III)/As(V) were quantified by the analytical methods described above.

Solid-phase As speciation was examined by As K-edge X-ray absorption near-edge structure (XANES) spectroscopy. Arsenic XANES data were collected using the XAS beamline at the Australian Synchrotron, as described previously.²¹ Fluorescence data (on samples diluted with cellulose to 0.1% As) were collected at 4 °K by a 100 element array Ge solid-state detector. The X-ray energy for each sample was calibrated against the first inflection point of the absorption edge of Au(0). Multiple scans of the same sample showed no change in As speciation due to beam damage. The relative abundance of As(III) and As(V) in selected solid-phase samples was quantified by linear combination fitting of XANES spectra against As(V) and As(III) reference standards.²¹

RESULTS

Field-Based Observations. The AMD flow-path at the study site can be divided into five zones, herein termed A, B, C, D, and E (Figure 1e). These zones display distinct differences in visible features, water quality characteristics, composition of ochreous precipitates, and mineralogical trends [i.e., Fe(III) mineral assemblages]. As such, the following sections present the results in a sequence that follows the AMD flow-path from zone A to zone E.

Zone A. The AMD flow-path originates as seepage from the base of a slimes (i.e., fine calcination waste) dam, which marks the start of zone A (Figure 1). At the time of sample collection, surface water in zone A had pH ranging from ~2.6 to ~2.8 and Eh from ~550 to ~700 mV (Figure 2). Samples of AMD from zone A contained high concentrations of SO_4^{2-} (up to 1990 mg L^{-1}), with relatively low concentrations of K^+ (~12 mg L^{-1}). This zone also contained high concentrations of total aqueous Fe (from 291 to 397 mg L^{-1}), which occurred predominantly as the Fe(II) species (Figure 3). Total aqueous As concentrations were also very high in zone A; spanning

10,100–32,400 $\mu\text{g L}^{-1}$ and comprising a mixture of both As(III) and As(V) (Figure 3).

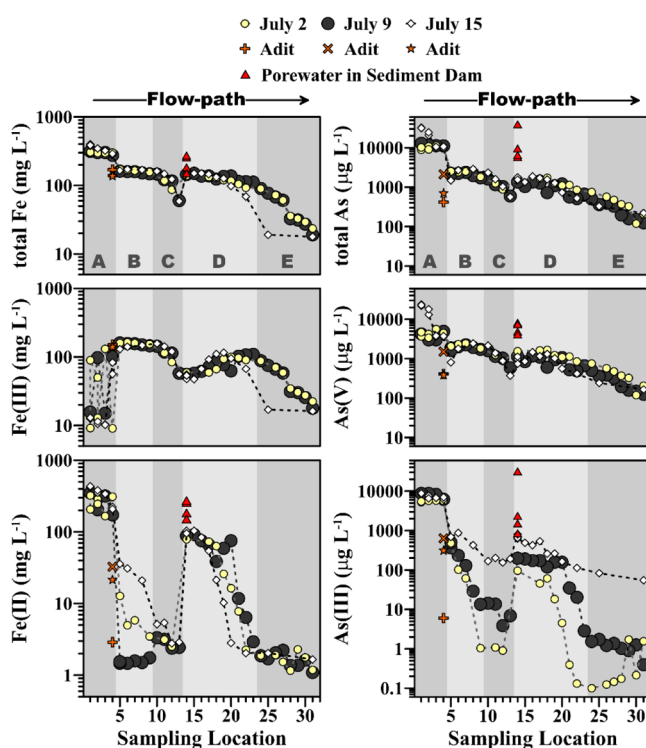


Figure 3. Variation in aqueous-phase total Fe, Fe(III), Fe(II), total As, As(V), and As(III) along the AMD flow-path at the study site. The letters, (A–E), denote the location of the five zones, as shown in Figure 1e, while the numbers on the horizontal axis denote the sampling location, as shown in Figure 1e. Note that in pore-water from the retention dam, total aqueous Fe was not significantly different from aqueous Fe(II) indicating negligible aqueous Fe(III).

Solid-phase precipitates in zone A were very pale yellow and occurred as hydrous suspensions forming in small pools or as more consolidated accumulations in terraces and drip-stones between pools (Supporting Information, Figure S2a,b). These precipitates contained total Fe concentrations that ranged from 225 to 273 g kg^{-1} and total As concentrations that ranged from 179 to 208 g kg^{-1} (Supporting Information, Table S1). The As K-edge XANES results show that >95% of total As in solid-phase samples from zone A occurred as As(V) (Figure 4). Less than 2.3 and 0.04% of total As occurred as surface-adsorbed (i.e., PO_4^{3-} -extractable) As(V) and As(III), respectively (Supporting Information, Table S1). Effectively all (>96%) of the total Fe and As in these precipitates were recovered by extraction with ammonium oxalate for 2 h at room temperature (Figure 5); with the exception of sample ZA-DrSt (a drip-stone accumulation) which had lower levels of Fe and As extractability (92 and 84%, respectively; Supporting Information, Table S1).

The XRD patterns for precipitates from zone A were characterized by two diffuse peaks centered at ~3.1 and ~1.6 Å, along with sharp peaks due to relatively minor jarosite and quartz (Figure 6a). The presence of two diffuse peaks is broadly similar to the well-known XRD profile of 2-line ferrihydrite. However, the position and shape of these peaks instead concur with previous reports for AFA.¹⁷ While obviously very rich in Fe and As, the AFA also contained an

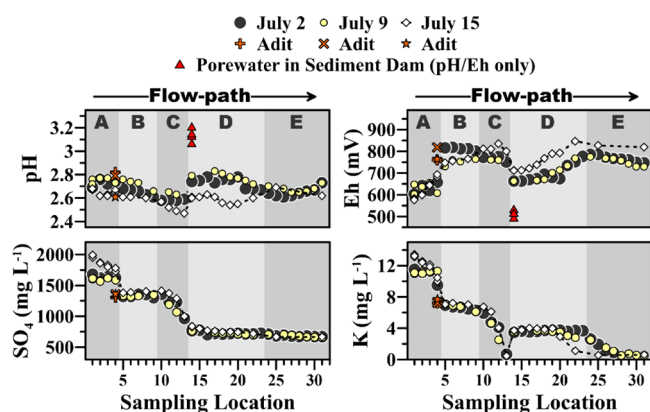


Figure 2. Variation in pH, Eh, and aqueous SO_4^{2-} and K^+ along the AMD flow-path at the study site. The letters, (A–E), denote the location of the five zones shown in Figure 1e, while the numbers on the horizontal axis denote the sampling location, as shown in Figure 1e.

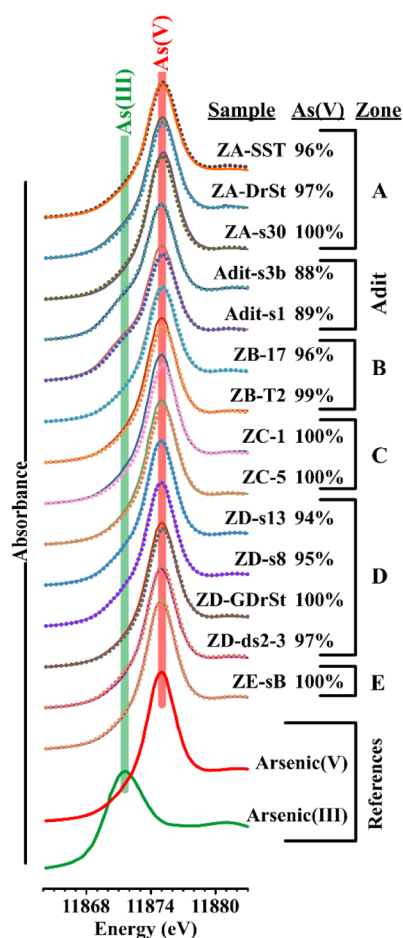


Figure 4. Arsenic K-edge XANES spectra for selected solid-phase samples from the study site in comparison to reference spectra for As(V) and As(III). The dashed lines denote sample data, while the corresponding solid line shows the least-squares best fit for a linear combination of As(V) and As(III). The labels to the right of each spectrum show the sample identification code with the corresponding relative abundance of As(V) as a % of total As. The R-factor for the linear combination fits ranged from <0.001 to 0.008.

appreciable S content (Supporting Information, Table S1), with molar Fe/S ratios of 4.7 to 6.5 (based on extraction with ammonium oxalate for 2 h at room temperature). SEM–EDX observations show that the AFA occurred as $\sim 1 \mu\text{m}$ spheroidal aggregations with a uniform micro-scale distribution of Fe, S, and As in ratios that are consistent with the bulk extraction-based ratios (Figure 7a).

The lower recovery of Fe and As by extraction with ammonium oxalate for 2 h at room temperature in the sample ZA-DrSt concurs with this sample containing larger amounts of jarosite than other samples from zone A. This is evident from both XRD patterns for the sample ZA-DrSt (Figure 6a) and its relatively high amount of K recovered by extraction with ammonium oxalate for 4 h at 80 °C (Supporting Information, Table S1). Differences in ammonium oxalate extractions for 4 h at 80 °C (which recovers both crystalline and poorly ordered phases³⁷) versus 2 h at room temperature (which recovers poorly ordered phases only³⁷) indicate that the jarosite in this sample had molar Fe/K, Fe/S and Fe/As ratios of 7.90, 1.88, and 6.80, respectively. The extraction results also indicate a molar Fe/(S + As) ratio of 1.48 which, in light of AsO_4^{3-} substitution for SO_4^{2-} within jarosite,³⁸ agrees closely with an

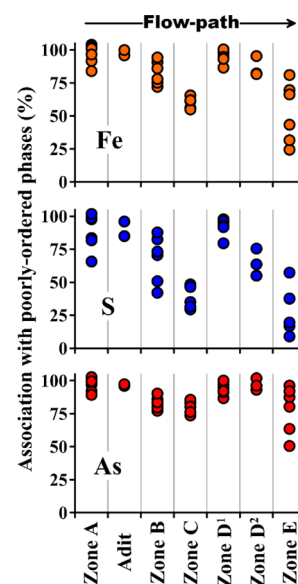


Figure 5. Variation in the percent of solid-phase Fe, S, and As associated with poorly ordered phases in ochreous precipitations forming along the AMD flow-path at the study site. The superscripts 1 and 2 for zone D refer to samples collected from pools vs those collected from terraces/drip-stones, respectively.

ideal molar Fe/(S + As) ratio of 1.5. Considered together, the molar ratios of crystalline As and S further indicate $\sim 22 \text{ mol } \%$ substitution of AsO_4^{3-} for SO_4^{2-} in jarosite within the sample ZA-DrSt.

The molar Fe/K ratio (7.90) within jarosite in the sample ZA-DrSt suggests a deficiency in K^+ relative to the K-jarosite end member (where the ideal molar Fe/K ratio = 3). This K^+ deficiency was not balanced by Na^+ , as would be expected for an intermediate between K- and Na-jarosite end members (i.e., Na^+ comprised only $\sim 5 \text{ mol } \%$ of the corresponding abundance of K^+ ; data not shown). The K^+ deficiency instead likely reflects significant incorporation of H_3O^+ . This accords with the XRD pattern for jarosite in the sample ZA-DrSt being well-matched by the reference XRD pattern provided by PDF 04-014-4654, which corresponds to an intermediate between the H_3O^- and K-jarosite end members.³⁹ Intermediates in the H_3O^- and K-jarosite series also typify the XRD patterns and crystalline Fe, K, and S ratios for precipitates collected from the other zones, as described below. For brevity, these intermediate phases are simply referred to herein as jarosite.

Adit Outflow. AMD discharged from zone A mixes with AMD released from an adit which sits between zone A and zone B (Figure 1). In comparison to zone A, AMD from the adit had a similar pH (2.6–2.8), a substantially higher Eh (750–820 mV), and lower concentrations of SO_4^{2-} and K^+ (Figure 2). The adit outflow also had lower total aqueous Fe concentrations compared to zone A (159–169 mg L^{-1}), which existed predominantly as the Fe(III) species (Figure 3). This dominance of aqueous Fe(III) over Fe(II) contrasts with zone A but is in accordance with the higher Eh in the adit outflow. The adit outflow also had total aqueous As concentrations (from 417 to 2130 $\mu\text{g L}^{-1}$) that were about an order of magnitude lower than those in zone A, and which existed mostly as the As(V) species (Figure 3).

The adit outflow area had reddish-yellow precipitates occurring as relatively consolidated accumulations on timber used to block access to the adit and which also acted as a weir

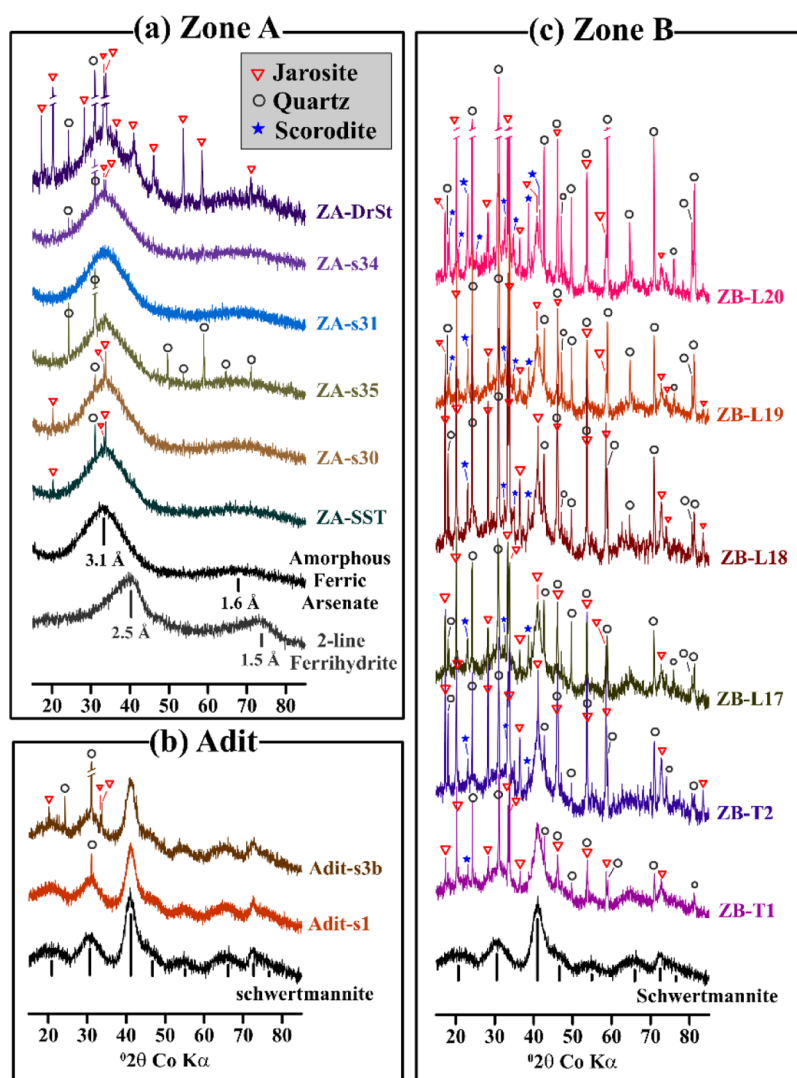


Figure 6. XRD patterns for samples collected from zone A (a), adit entrance (b), and zone B (c). XRD patterns for synthetic AFA, 2-line ferrihydrite, and schwertmannite are also presented to assist interpretation. The labels to the right of each XRD pattern denote the sample identification code (or the identity of synthetic phases).

that slowed water outflow from the adit (Figure 1c). In comparison to the AFA-rich precipitates in zone A, precipitates at the adit entrance contained higher total Fe concentrations (380–390 g/kg) and lower, but still very high, total As concentrations (13.0–26.7 g kg⁻¹) (Supporting Information, Table S1). The vast majority of As (close to 90%) was found to be present as As(V), according to As K-edge XANES spectroscopy (Figure 4). Only 0.64–1.3 and 0.05–0.10% of total As occurred as surface-adsorbed (i.e., PO₄³⁻-extractable) As(V) and As(III), respectively (Supporting Information, Table S1). The precipitates were predominantly poorly ordered, with >95% of total Fe and As being recovered by extraction with ammonium oxalate for 2 h at room temperature (Figure 5). The XRD patterns reflect this poorly ordered nature, showing that the material was principally composed of schwertmannite along with some very minor jarosite and quartz (Figure 6b). SEM observations confirm the presence of schwertmannite in its distinctive ball-and-whisker micromorphology (Figure 7b), with micro-scale molar Fe/S and molar Fe/As ratios that generally concur with those based on the extraction results (i.e., molar Fe/S ratios of 4.5–5.0 and molar Fe/As ratios of 19–37).

Zone B. The pH, Eh, and general composition of surface water at the upstream end of zone B were consistent with a mixture of AMD from zone A and from the adit outflow (Figure 2). The pH, Eh, and aqueous SO₄²⁻ and K⁺ concentrations (Figure 2), in addition to aqueous total Fe and total As remained relatively constant across zone B (Figure 3). In contrast, the aqueous Fe(II) and As(III) concentrations decreased substantially, dropping to as low as ~1.5 mg L⁻¹ and ~1 μg L⁻¹, respectively (Figure 3).

Ochreous precipitates in zone B occurred as encrustations on recalcitrant leaf litter in pools and as consolidated accumulations in terraces between pools. The total Fe and As concentration in these precipitates ranged from 189 to 382 and 17.6 to 31.5 g kg⁻¹, respectively (Supporting Information, Table S1). Greater than 95% of total solid-phase As occurred as the As(V) oxidation state (Figure 4). Less than 3% of total As was surface adsorbed (i.e., PO₄³⁻-extractable), with almost all of this adsorbed As occurring as the As(V) species (Supporting Information, Table S1). A lower percentage of total Fe and As (72–94 and 77–90%, respectively) was recovered by extraction with ammonium oxalate for 2 h at room temperature from zone B samples in comparison to the

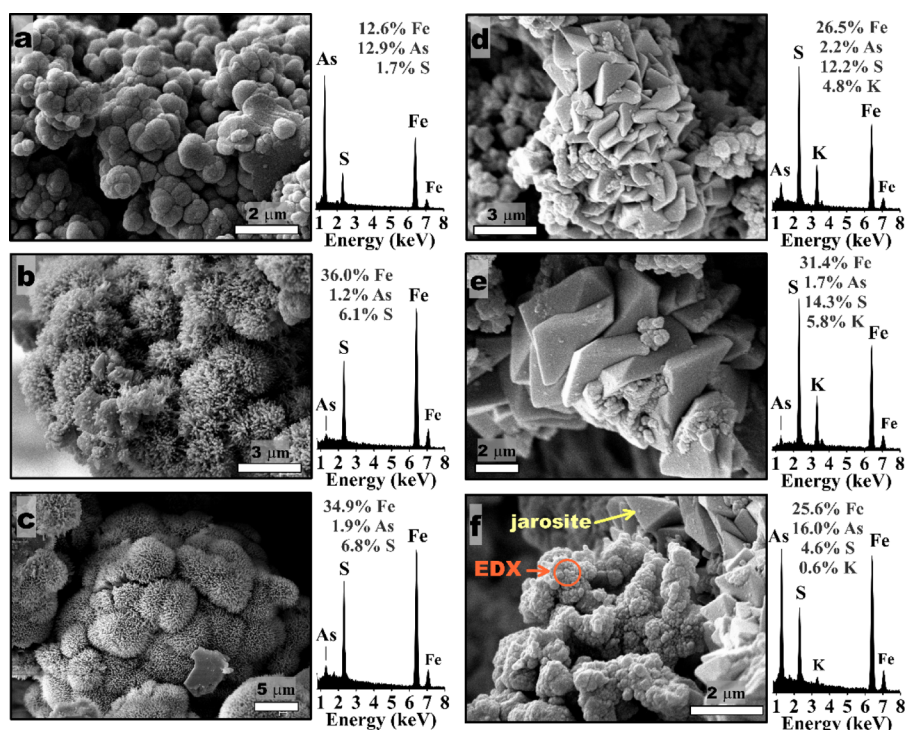


Figure 7. SEM and EDX spectra showing micromorphology and composition, respectively, of (a) AFA in sample ZA-s30 from zone A, As-bearing schwertmannite in (b) sample adit-1 collected from the adit entrance and in (c) sample ZD-s13 from zone D, As-bearing jarosite in (d) sample ZB-s19 from zone B and in (e) sample ZC-s1 from zone C, and (f) As- and Fe-rich material in close proximity to jarosite in sample ZD-DS2c from zone D.

AFA-dominant precipitates in zone A and the schwertmannite-dominant precipitates at the adit entrance (Figure 5). This reflects the presence of more substantial amounts of highly crystalline jarosite, along with some minor scorodite, in zone B samples as evident from the XRD (Figure 6c) and SEM–EDX observations (Figure 7d). The abundance of jarosite in these samples is further evident from the zone B samples containing higher amounts of K extracted by ammonium oxalate at 80 °C for 4 h than samples from zone A or from the adit entrance area (Supporting Information, Table S1).

The XRD patterns for samples from zone B also show abundant schwertmannite, which contributed its distinct pattern of eight diffuse peaks to the XRD baseline (Figure 6c). The oxalate extraction results (2 h at room temperature; Supporting Information, Table S1) suggest that this schwertmannite had a molar Fe/S ratio of 4.3–5.6 and a corresponding molar Fe/As ratio of 7.0–25.

Zone C. In this zone, the AMD flow-path traverses waste rock (Figure 1) upon which Fe(III) phases appeared to have formed a surface hard-pan layer. In general, as AMD flows across zone C, Eh remained relatively constant at ~750 to ~850 eV, while pH decreased slightly (down to a minimum near pH 2.4) along with decreases in the aqueous concentrations of SO_4^{2-} and K^+ (Figure 2). Total aqueous Fe and As concentrations also diminished in zone C (to between 59–84 and 561–595 $\mu\text{g L}^{-1}$, respectively), and both existed mainly as their most oxidized species; Fe(III) and As(V) (Figure 3).

The relatively well-cemented Fe(III) phases in the surface hardpans in zone C contained total Fe at 349–391 g kg^{-1} and total As at 20.5–39.1 g kg^{-1} . Arsenic K-edge XANES spectroscopy indicated that solid-phase As in samples from zone C existed entirely as As(V) (Figure 4), with surface-

adsorbed (i.e., PO_4^{3-} -extractable) As(V) making up <2% of total As (Supporting Information, Table S1). In contrast to the upstream zones, only 55–66% of total Fe and 73–85% of total As were recovered by extraction with ammonium oxalate for 2 h at room temperature (Figure 5). This reflects a trend of decreasing abundance of poorly ordered phases and increasing abundance of crystalline As-rich Fe(III) phases as AMD flows from zone A to zone C.

In accordance with this trend in extraction behavior, the XRD patterns show a relative abundance of jarosite in zone C compared to the previously described upstream zones (Figure 8a). Electron microscopy confirmed the presence of highly crystalline jarosite in samples from zone C as mainly pyramidal rhombs in the ~2 to ~5 μm size range (Figure 7e). Enlargement of the lower intensity peaks in the XRD patterns, as shown in Figure 8a, reveals that a minor amount of the crystalline Fe(III) also occurred in the form of scorodite. The XRD baseline, as shown in Figure 8a, indicates that the zone C precipitates also contained schwertmannite. Extraction with ammonium oxalate for 2 h at room temperature suggests that the schwertmannite in zone B had molar Fe/S ratios of 5.3–5.8 and molar Fe/As ratios of 10.1–16.5.

Zone D. AMD flows into zone D via a sediment retention pond (Figure 1), which contained up to about 0.4 m of surface water overlaying abundant leaf litter and associated organic-rich sediment. Surface water in the sediment retention pond displayed an increase in pH by ~0.2 to ~0.3 units (climbing to pH ~ 2.8) and a decrease in Eh by ~100 mV (dropping to ~650 to ~700 mV) in comparison to the nearest upstream sample location in zone C (Figure 2). This shift in pH/Eh was matched with substantial increases in the surface water concentrations of aqueous Fe(II) and As(III) (Figure 3). Examination of sediment pore-water from the sediment

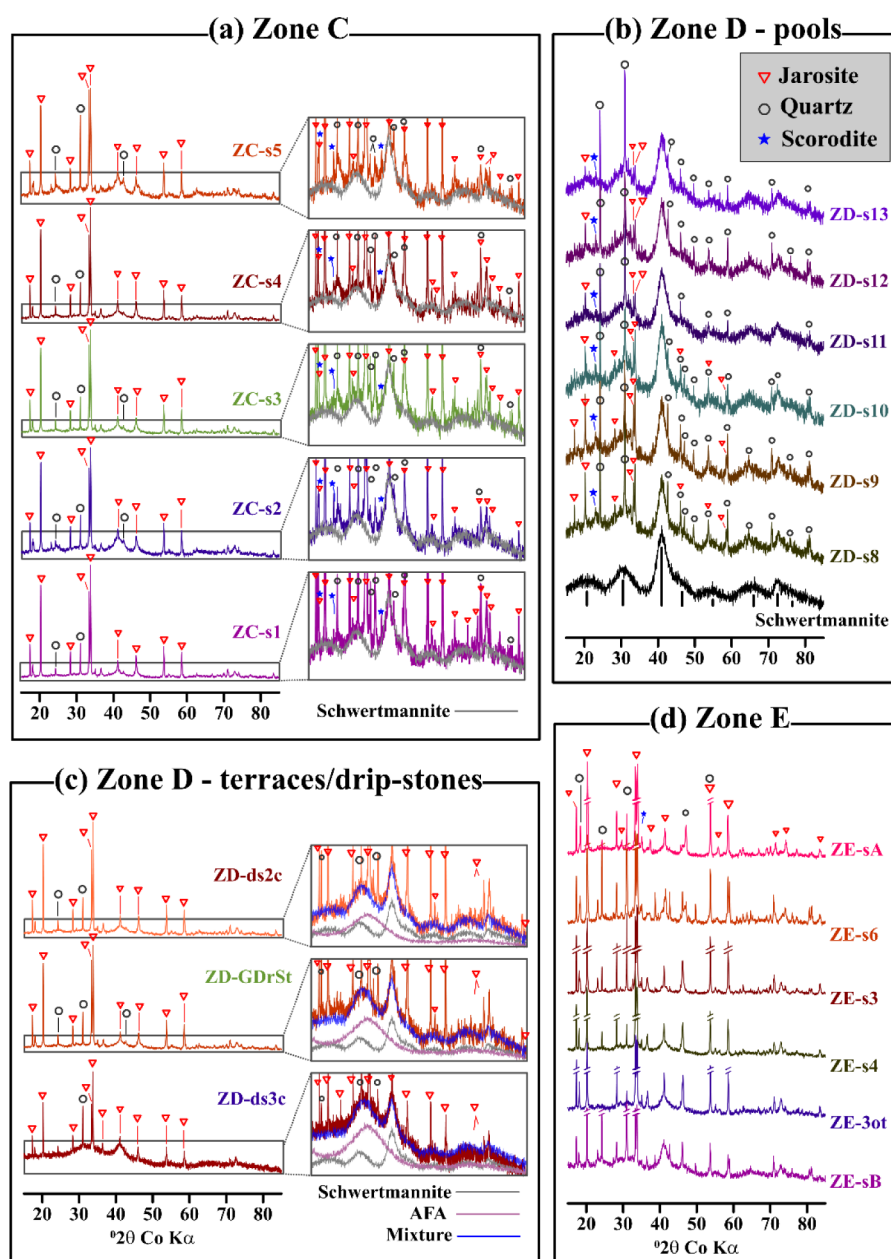


Figure 8. XRD patterns for samples from (a) zone C, (b) pools in zone D, (c) terraces/drip-stones in zone D, and (d) zone E. The enlarged patterns on the right-hand side of (a) indicate the presence of schwertmannite (i.e., as evident from comparison against the overlaid XRD pattern of synthetic schwertmannite, shown in gray). The enlarged patterns on the right-hand side of (c) indicate the presence of both schwertmannite and AFA (i.e., as evident from comparison against the overlaid XRD pattern of calculated mixtures of synthetic AFA and synthetic schwertmannite, with AFA/schwertmannite ratios of 5:5, 4:6, and 3:7 for ZD-ds3c, ZD-GDrSt, and ZD-ds2c, respectively). The labels to the right of each XRD pattern denote the sample identification code.

retention pond revealed the development of higher pH (3.0–3.2) and more reducing conditions ($E_h = 500\text{--}550$ mV) below the sediment–water interface (Figure 2). This coincided with high pore-water concentrations of Fe(II) ($131\text{--}228$ mg L⁻¹), As(V) ($3850\text{--}7570$ μg L⁻¹), and As(III) ($794\text{--}29,600$ μg L⁻¹) (Figure 3).

Downstream of the sediment retention pond, pH within zone D remained relatively constant between ~ 2.5 and ~ 2.8 , while E_h climbed steadily to between ~ 750 and ~ 850 mV (Figure 2). This increase in E_h was mirrored by increases in aqueous Fe(III) and corresponding decreases in aqueous Fe(II), which diminished by almost 2 orders of magnitude across zone D (Figure 3). The aqueous As concentrations also

decreased across zone D, with aqueous As(III) declining by between ~ 1 and ~ 3 orders of magnitude between the sediment retention pond and the end of zone D, compared to less substantial decreases in aqueous As(V) (Figure 3).

Zone D had particularly prominent accumulation of reddish-yellow ochreous precipitates (Supporting Information, Figure S2c–f). These precipitates occurred as encrustations on leaf litter and rocks within pools and as relatively well-consolidated cemented terraces or drip-stones in high-flow areas. Total Fe concentrations were similar for material occurring in both pools and terraces/drip-stones, ranging from 310 to 370 g kg⁻¹ (Supporting Information, Table S1). In contrast, total As concentrations were considerably lower in the ochreous

encrustations formed in pools (14.0–20.3 g kg⁻¹) compared to the well-consolidated terrace/drip-stone material (47.5–67.9 g kg⁻¹). Between 87 and 100% of As and 82 and 100% of Fe in zone D samples were associated with poorly ordered phases, which represents a jump in the proportional abundance of such phases from zone C to zone D (Figure 5). Like the other zones, the vast majority (94–100%) of solid-phase As was present as the As(V) oxidation state (Figure 4) with only a very small proportion (<3%) of total As occurring as surface-adsorbed As(V) (i.e., PO₄³⁻-extractable) (Supporting Information, Table S1).

The XRD patterns, as shown in Figure 8b,c, reveal distinct differences between precipitates in pools versus terraces/drip-stones, respectively. The XRD patterns for material collected from pools in zone D show a dominance of schwertmannite, with only relatively minor jarosite and quartz (Figure 8b). The SEM–EDX examination of pool samples from zone D confirmed the presence of schwertmannite with distinct ball-and-whisker morphology (Figure 7c). Extraction with ammonium oxalate for 2 h at room temperature suggests that schwertmannite in these samples contained molar Fe/S ratios ranging from 4.7 to 5.0 and molar Fe/As ratios ranging from 23.5 to 35.1.

In contrast, the XRD patterns for terrace/drip-stone samples from zone D were dominated by prominent jarosite peaks (Figure 8c). Enlargement of the XRD baseline pattern for these samples reveals that they also contained a mixture of AFA and schwertmannite. The SEM–EDX examination suggests that the AFA/schwertmannite in these samples occurred as aggregations of nanocrystallites with relatively low molar Fe/As ratios (down to ~2) (Figure 7f). These AFA/schwertmannite aggregates occurred in close proximity to larger jarosite crystals which had much higher molar Fe/As ratios (from ~17 to ~25).

The presence of AFA in terrace/drip-stone samples from zone D is consistent with their relatively high total As content, as well as their lower molar ratio of Fe/As (6.0–9.0) in ammonium oxalate (2 h at room temperature) extractions compared to the corresponding molar ratios (Fe/As > 23) in the samples collected from pools (Supporting Information, Table S1). The prominence of jarosite in terrace/drip-stone samples also concurs with their greater crystalline K and S content compared with samples collected from pools (based on extraction with ammonium oxalate for 4 h at 80 °C) (Supporting Information, Table S1).

Zone E. Surface water across zone E remained very acidic (pH ~ 2.6–~2.7) and oxidizing (Eh ~ 700–~800 mV), with aqueous SO₄²⁻ remaining at a relatively constant concentration of ~600 mg L⁻¹ (Figure 2). In contrast, aqueous K⁺ displayed a trend of decreasing concentrations toward the end of zone E (Figure 2). Total aqueous Fe also decreased across zone E (dropping to between 17.8 and 22.4 mg L⁻¹; Figure 3) as did total aqueous As (dropping to between 206 and 219 μg L⁻¹; Figure 3). Throughout zone E, aqueous Fe and As existed mainly as the Fe(III) and As(V) species, respectively.

Zone E contained no particularly obvious in-stream accumulation of Fe(III) precipitates. Nevertheless, this zone did contain accumulations of abundant Fe(III) materials in stranded terraces and as cemented accumulations on exposed rocks. The XRD examination of these materials showed jarosite along with some schwertmannite with minor scorodite (Figure 8d). The total Fe and As concentration in these precipitates ranged from 213 to 338 and 18.7 to 42.6 g kg⁻¹,

respectively (Supporting Information, Table S1). In general, lower percentages of total Fe and As (24–81 and 50–96%, respectively) were recovered by extraction with ammonium oxalate for 2 h at room temperature from zone E samples compared to upstream samples in zone D (Figure 5). This accords with an increased abundance of jarosite in precipitates from zone E, as reflected in corresponding increases in the concentrations of K and S recovered from crystalline phases (Supporting Information, Table S1).

Arsenic Enrichment and Fe Mineralogy across All Zones. Figure 9 presents the relationship between molar Fe/

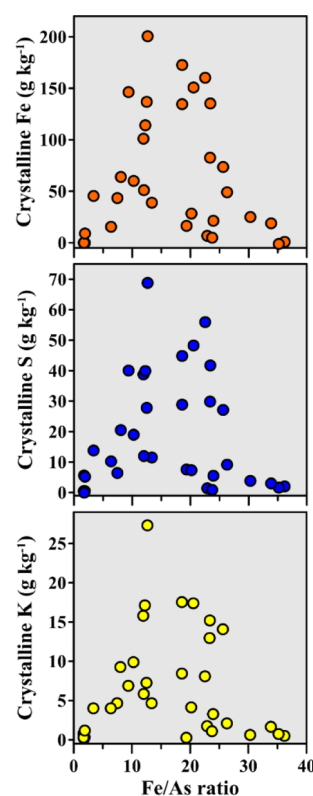


Figure 9. Relationship between crystalline Fe, S, and K (which can be considered to be proxies for jarosite abundance in this study) and the corresponding molar Fe/As ratio in ochreous precipitates formed from AMD at the study site.

As ratios in solid-phase samples from all zones and the corresponding concentrations of crystalline Fe, S, and K (defined as the difference in element abundance between ammonium oxalate extractions conducted for 4 h at 80 °C minus parallel extractions conducted for 2 h at room temperature). In this study, the crystalline Fe, S, and K concentrations can be considered as reasonable proxies for the abundance of jarosite (given that jarosite was the predominant crystalline Fe, S, and K host-phase in the samples examined here). The relationships depicted in Figure 9 therefore show that jarosite was most abundant in samples having intermediate molar Fe/As ratios. When considered along with the XRD patterns described above, it appears that high molar Fe/As ratios [i.e., relatively low As concentrations in Fe(III) phases] are associated with samples having little jarosite but an abundance of schwertmannite. Low molar Fe/As ratios [i.e., high As concentrations in Fe(III) phases] are also associated with samples having little jarosite. However, in these relatively

As-rich samples, there is little or no schwertmannite, with Fe(III) phases instead occurring predominantly as AFA.

Laboratory-Based Experimentation: Mineral Formation. The initial solid-phase material produced in the mineral formation experiment dissolved entirely during extraction with ammonium oxalate for 2 h at room temperature. This extractability accords with the XRD patterns which show the presence of only schwertmannite and/or AFA (Figure 10). At

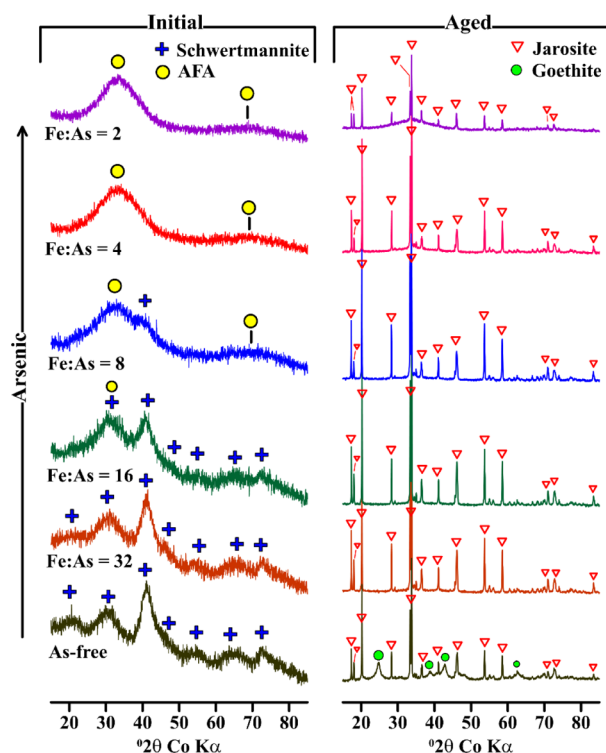


Figure 10. XRD patterns for (left side panel) the initial solid phase in the mineral formation experiment and (right side panel) the final solid phase resulting from aging of the initial material (10 days at 60 °C).

the lowest As(V) levels examined here [i.e., Fe/As = 32 and As(V)-free treatments], the XRD patterns suggest that schwertmannite was the only solid-phase to form initially. Conversely, in the presence of the largest amounts of As(V) examined here (i.e., treatments having molar Fe/As ratios of 2 and 4), the XRD patterns show only two diffuse peaks indicating the presence of AFA. At intermediate As(V) levels (i.e., molar Fe/As ratios of 8 and 16), the XRD patterns suggest that the initial solid-phase comprised a mixture of both schwertmannite and AFA. Overall, the results of the mineral formation experiment show that schwertmannite formation was inhibited at higher As(V) concentrations, which instead favored the formation of AFA (Figure 10).

Laboratory-Based Experimentation: Mineral Transformation. Aging of the schwertmannite and AFA suspensions led to the formation of crystalline Fe(III) phases (Figure 10). Under As-free conditions, these crystalline phases included both jarosite and goethite. In contrast, in the presence of As(V), jarosite was the only crystalline phase to form from precursor AFA and schwertmannite. Aging of these As(V)-bearing precursor phases for 10 days at 60 °C produced jarosite which had molar Fe/(As + S) ratios of between 1.42 and 1.59 (from data presented in Supporting Information, Table S2). These ratios agree closely with an expected

stoichiometric molar Fe/(S + As) ratio of 1.5 (considering possible AsO_4^{3-} substitution for SO_4^{2-} in pure jarosite, where the molar Fe/S ratio = 1.5). Examination of the crystalline As and S concentrations indicates that the highest observed molar As/(As + S) ratio in material aged for 10 days was 0.21 (which equates to 21 mol % substitution of AsO_4^{3-} for SO_4^{2-} in jarosite produced via transformation of AFA in the molar Fe/As = 2 treatment).

Interestingly, the greatest levels of jarosite formation (based on XRD peak height as well as the crystalline K and S concentrations) occurred at intermediate Fe/As ratios (Figure 11). This was particularly noticeable after aging for only 2 days

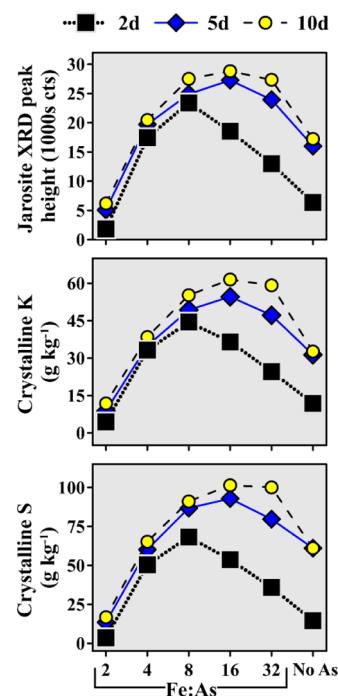


Figure 11. Relative abundance of jarosite, approximated by XRD peak height and crystalline K and S concentrations, as a function of the molar Fe/As ratio during aging (2, 5, and 10 days at 60 °C) of suspensions from the mineral formation experiment. The XRD peak height refers to the (012) peak for jarosite centered at $\sim 21^\circ 2\theta$ Co K α . Association with crystalline phases was calculated as the difference between K and S extracted by ammonium oxalate for 4 h at 80 °C minus 2 h at room temperature (in the dark).

at 60 °C, where jarosite formation was greatest at a molar Fe/As ratio of 8, with progressively less jarosite forming at lower and higher Fe/As ratios (Figure 11). This trend was also apparent in the solid-phase Fe extraction data, which revealed that $\sim 60\%$ of solid-phase Fe occurred in the form of jarosite by day 2 at molar Fe/As = 8, compared to $<10\%$ in the corresponding As-free and molar Fe/As = 2 treatments [i.e., the lowest and highest levels of As(V) examined here] (Figure 12). Like jarosite-bound Fe, maximal levels of jarosite-bound As also occurred at intermediate molar Fe/As ratios (Figure 12). In this case, the greatest percentage of jarosite-bound As at 2 days (i.e., 17% of solid-phase As) occurred at a molar Fe/As ratio of 8, while by 10 days, this had shifted to a molar Fe/As ratio of 16 (and increased to 32% of solid-phase As).

The oxalate extraction results indicate that As(V) was preferentially bound within poorly ordered phases (schwertmannite and AFA), relative to its corresponding incorporation

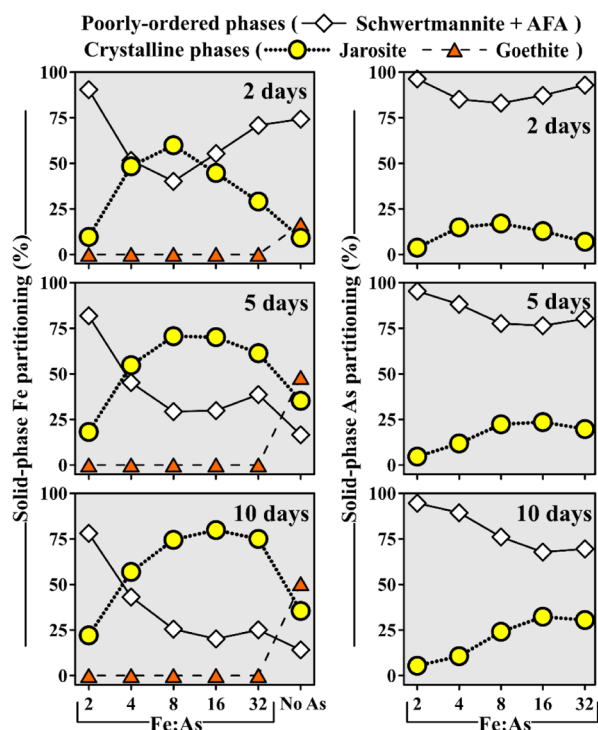


Figure 12. Partitioning of solid-phase Fe and As between poorly ordered phases (AFA + schwertmannite) and crystalline phases (jarosite or goethite) as a function of the molar Fe/As ratio during aging (2, 5, and 10 days) at 60 °C of suspensions from the mineral formation experiment. Association with jarosite [which XRD showed was the only crystalline phase in treatments where As(V) was present] was calculated as the difference between Fe and As extracted by ammonium oxalate for 4 h at 80 °C minus 2 h at room temperature (in the dark) in treatments where As(V) was present. The abundance of jarosite-bound Fe in the As-free treatment (where goethite was also present) was calculated from the crystalline K concentration and assuming a molar Fe/K ratio of 3 in jarosite (which is reasonable given an excess supply of K⁺ in this experiment). The abundance of goethite-Fe in this treatment was calculated as crystalline Fe minus jarosite-bound Fe.

within jarosite (Figure 12). In comparison to solid-phase Fe (e.g., where up to 80% of Fe was jarosite-bound at day 10), solid-phase As exhibited a much lower tendency for incorporation within jarosite (e.g., up to only 32% of As was jarosite-bound at 10 days). This comparison shows that despite extensive jarosite formation and considerable uptake of As(V) by jarosite, both schwertmannite and AFA remained as preferential host phases for As(V). This preferential hosting of As(V) by schwertmannite and AFA is further reflected in the molar Fe/As ratios at 10 days ranging from 1.6 to 12.2 in poorly ordered phases (AFA and schwertmannite, respectively) compared to corresponding ratios of 7.8–83 for jarosite (based on extraction data shown in Supporting Information, Table S2). These ratios demonstrate that both schwertmannite and AFA were substantially enriched in As(V) relative to jarosite.

DISCUSSION

Mobilization of As and Fe under Oxidizing Conditions. Arsenopyrite and arsenian pyrite are the most common primary sources of As in wastes produced from mining and associated processing activities.³ These sulfide minerals are unstable under oxidizing conditions, and their oxidation in carbonate-poor mining waste releases acidity as

well as aqueous As, Fe, and SO₄²⁻. Oxidative dissolution of arsenopyrite and arsenian pyrite occurs via a series of microbially mediated and abiotic steps, initially yielding aqueous As(III) and Fe(II).³ This can lead to the formation of strongly acidic, As(III)- and Fe(II)-rich AMD, as observed in zone A at the study site. With further oxidation, aqueous As(III) and Fe(II) are progressively replaced by As(V) and Fe(III), which is consistent with the general trend in aqueous As and Fe speciation along the AMD flow-path described here.

Mobilization of As and Fe under Reducing Conditions. In addition to oxidative dissolution, mobilization of Fe and As can also occur via microbially mediated reductive dissolution of secondary As-bearing Fe(III) minerals.^{18,40} This may involve Fe(III)-minerals formed directly within mine wastes (e.g., in flooded tailings or waste rock) or formed from the AMD released from such wastes. The sediment retention pond in zone D provides an example of reductive dissolution of As-bearing Fe(III) minerals in an AMD system. Organic-rich, waterlogged conditions in the sediments accumulated within this pond have created pH–Eh conditions that are strongly favorable for microbial Fe(III)-reduction and consequent release of aqueous Fe(II) and co-associated As (Supporting Information, Figure S3 provides a pH–Eh stability field diagram, generated using the Thermoddem database⁴¹). When considered in terms of As speciation, the pH–Eh data for pore-water in the sediment retention pond sit within the stability field for aqueous As(V) (i.e., H₂As^VO₄⁻) (Supporting Information, Figure S3). However, lower Eh favors some reduction of As(V) to As(III), given the close proximity of the pore-water pH–Eh data to the field of predominance for As^{III}(OH)₃O (Supporting Information, Figure S3).

Formation of As-Rich Fe(III) Minerals. Whether released via oxidative or reductive dissolution pathways, aqueous Fe(II) is oxidized in surface water to Fe(III), thereby leading to the formation of a series of Fe(III) minerals. The aqueous- and solid-phase results provide evidence that formation of these minerals drives removal of aqueous As from AMD at the study site. The results show that <3% of total As in Fe(III) minerals collected from AMD was surface adsorbed (i.e., PO₄³⁻-extractable), indicating that As was retained predominantly by incorporation within the Fe(III) mineral structure.

Incorporation of As into the structure of the minerals observed in this study can be attributed to coprecipitation of As(V) with Fe(III). This enables levels of As enrichment within Fe(III) minerals that far exceed the corresponding levels that are possible by surface adsorption alone. Accordingly, Fe(III) minerals in AMD at the study site contained very high As concentrations (13–208 g kg⁻¹) and were limited to phases which are capable of structurally accommodating substantial amounts of As(V). This includes AFA and scorodite where As^VO₄ is a necessary component of the crystal structure, as well as schwertmannite and jarosite where As^VO₄ is not essential to the crystal structure but is incorporated as a substitute for structural SO₄ (as discussed in detail below).

Amorphous Ferric Arsenate. AFA was identified, based on two broad XRD peaks centered at 3.1 and 1.6 Å combined with its Fe- and As-rich composition,¹⁷ as the main Fe(III) phase occurring in zone A. It should be noted that AFA has also been commonly referred to as hydrous ferric arsenate, amorphous scorodite, and As-rich hydrous ferric oxide (As–HFO).^{3,10,42–46} Sulfate-rich AFA, as described in the present study, has been referred to as amorphous iron sulfoarsenates, AFA sulfate, and pitticite—a mineral name of questionable

validity that applies to amorphous $\text{Fe}_x(\text{AsO}_4)_y(\text{SO}_4)_z \cdot n\text{H}_2\text{O}$ phases having no consistent stoichiometry.^{12,17} Agreement on the atomic structure of AFA also remains elusive, with views divided between a “framework” structure similar to scorodite and a “chain” structure similar to butlerite $[\text{Fe}^{\text{III}}(\text{SO}_4)(\text{OH}) \cdot 2\text{H}_2\text{O}]$ and fibroferrite $[\text{Fe}^{\text{III}}(\text{SO}_4)(\text{OH}) \cdot 5\text{H}_2\text{O}]$.^{36,44}

The AFA from zone A had molar Fe/As ratios ranging from 1.7 to 3.0, which is higher than the ideal ratio of 1.0 in pure synthetic AFA. These ratios are comparable to the results for AFA produced in our mineral formation experiment [i.e., molar Fe/As = 1.8 and 2.3 at the two highest levels of As(V) addition, where AFA was the only phase according to XRD]. The ratios indicate an enrichment in Fe relative to As, which is consistent with previous studies of AFA from a range of environments. For example, naturally occurring AFA from marine hydrothermal vents (described as “As–HFO”) was found to have a molar Fe/As ratio of ~ 4 . Inskeep et al.⁴² report a molar Fe/As ratio of ~ 1.6 in AFA from acidic geothermal springs in Yellowstone National Park, USA. In As-rich AMD systems, which are comparable to the study site examined here, AFA has been found to have molar Fe/As ratios ranging from ~ 1.1 to ~ 2.5 .^{11,12,47}

Our field-based observations of AFA occurrence are consistent with the results from our laboratory-based mineral formation experiment. This experiment showed that high As(V) concentrations, as occurred in zone A, favored the formation of AFA over schwertmannite following Fe(II) oxidation under acidic, SO_4^{2-} -rich conditions. These results agree with previous abiotic mineral synthesis experiments by Carlson et al.¹¹ and Regenspurg and Peiffer.³⁰ These researchers found that forced hydrolysis of acidic SO_4^{2-} -rich $\text{Fe}^{\text{III}}\text{Cl}_3$ solutions at 60 °C in the presence of low As(V) concentrations led to schwertmannite formation, whereas high As(V) concentrations led to AFA formation. Our results also concur with Maillot et al.¹² who found that AFA was formed instead of schwertmannite below a molar Fe/As ratio of 5 [in an experiment involving forced hydrolysis at 80 °C of $(\text{Fe}^{\text{III}})_2(\text{SO}_4)_3$ solutions in the presence of varying As(V) concentrations]. Preferential AFA formation under As(V)-rich conditions reflects the strong affinity of the AsO_4 tetrahedron for rapid binding to FeO_6 octahedra, which hinders development of edge-sharing linkages between FeO_6 octahedra needed for schwertmannite nucleation.¹²

The dominance of AFA in zone A at the study site also concurs with the pH- and As(V)-dependent stability fields, as shown in Figure 13a. Using representative AMD conditions at the study site, Figure 13a shows that, at pH 2.4–2.8, aqueous As(V) activities above $\sim 10^{-4.5}$ (i.e., above $\sim 2400 \mu\text{g L}^{-1}$) thermodynamically favor AFA over schwertmannite. Schwertmannite is favored over AFA at lower As(V) activities but is metastable with regard to jarosite at these lower As(V) activities when pH is below ~ 3 (Figure 13b). It is noteworthy that the only data points sitting in the AFA field in Figure 13b are those from zone A, where AFA was indeed found to be the dominant phase.

Interestingly, despite much lower surface water As(V) concentrations, AFA was also present in some samples collected from zone D (Figure 8c). These samples were from material that occurred in either drip-stones on the wall of the sediment retention pond or from terrace-like accumulations developed on logs which formed small natural dams in the AMD flow-path. A feature of these AFA-bearing accumulations is that they likely received some diffusive flux

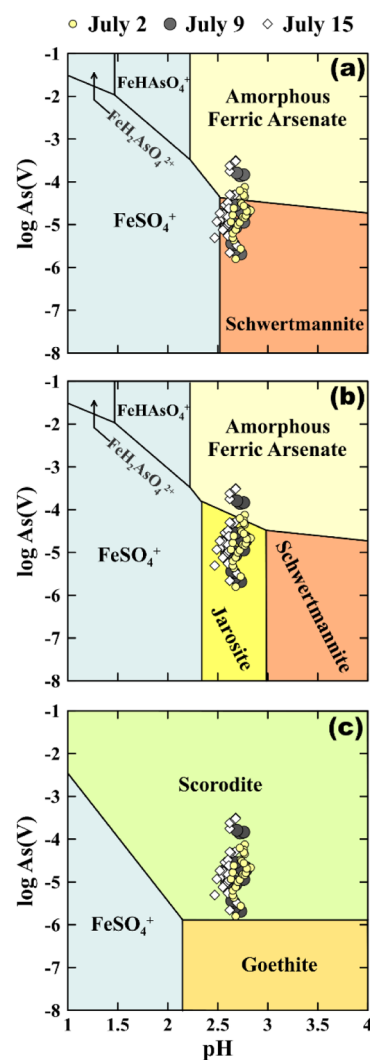


Figure 13. pH–As stability field diagram for Fe in the Fe–K–As–S– H_2O system at 10 °C and 1 bar for representative AMD composition ($\text{Fe}^{3+} = 10^{-3.0}$; $\text{K}^+ = 10^{-3.5}$; and $\text{SO}_4^{2-} = 10^{-2}$) at the study site in comparison to results for pH and aqueous As(V). The three diagrams show the successive distribution of phases as progressively more stable phases are considered from (a–c). Jarosite, goethite, scorodite, and hematite are suppressed in (a); goethite, scorodite, and hematite are suppressed in (b), and only hematite is suppressed in (c). Stability fields were calculated using thermodynamic constants from the Thermoddb database.⁴¹

of reducing pore-water (e.g., as occurred in the sediment retention pond). The results show that mildly reducing conditions in pore-water can produce relatively high aqueous As(V) concentrations (Figure 3 and Supporting Information, Figure S3), as a result of reductive dissolution of As(V)-bearing Fe(III) minerals [note that Fe(III) reduction occurs at a higher Eh than As(V) reduction, as shown in Figure S3 in Supporting Information]. This localized enrichment in aqueous As(V) may therefore explain the occurrence of AFA in zone D terrace/drip-stone material.

Schwertmannite. Schwertmannite was the main phase in ochreous precipitates formed at the adit entrance and in pools downstream of the sediment retention pond and was a major phase in all other samples downstream of zone A at the study site. Schwertmannite is a nanocrystalline Fe(III) oxyhydroxy-sulfate mineral that is perhaps the most common direct

precipitate of Fe(III) from acid-sulfate waters in the pH range of 2–4.^{48,49} As such, it has been widely documented in acid-sulfate environments, including metalliferous mine drainage,^{5,6,15,25,50,51} coal mine drainage,^{14,52–56} mine pit lakes,^{57–60} and acid-sulfate soils.^{61–65}

While some may disagree,⁶⁶ the structure of schwertmannite is generally thought to be analogous to a distorted akaganeite (FeOOH) unit cell where double chains of edge-sharing FeO₆ octahedra share corners, thereby forming tunnels.^{48,67} In akaganeite, the tunnel cavities are occupied and stabilized by Cl⁻, F⁻, or OH⁻, whereas SO₄²⁻ plays this essential stabilizing role in schwertmannite.⁵² Although schwertmannite has an ideal formula of Fe₈O₈(OH)₆SO₄·*n*H₂O, its actual composition is variable and described by Fe₈O₈(OH)_{8-2*x*}(SO₄)_{*x*}·*n*H₂O, where *x* varies between 1 and 2.^{53,54,68} This composition range implies molar Fe/S ratios of between 4 and 8, which bracket the variability in molar Fe/S ratios (4.3–6.5) observed in poorly crystalline phases in AMD at the study site.

Several authors have found that AsO₄³⁻ can be incorporated into schwertmannite by substitution for SO₄²⁻.^{4,11,30,69–71} In the present study, the extent of this AsO₄³⁻-for-SO₄²⁻ substitution is reflected in molar As/(As + S) ratios spanning 0.11–0.38 in ammonium oxalate extracts (2 h at room temperature) of samples from the study site which contained schwertmannite but showed no evidence of AFA presence (Supporting Information, Figure S5a). The observed range in molar As/(As + S) ratios suggest an upper limit of AsO₄³⁻ substitution for SO₄²⁻ in schwertmannite of ~40 mol %. This field-based data agree rather well with laboratory-based schwertmannite formation experiments, as described by Carlson et al.¹¹ and Regenspurg and Peiffer.³⁰ These researchers found that synthetic schwertmannite [formed via Fe(III) hydrolysis at 60 °C in the presence of AsO₄³⁻ and SO₄²⁻] could accommodate up to ~45 mol % substitution of AsO₄³⁻ for SO₄²⁻ without notable changes in the XRD pattern.

Schwertmannite is metastable, with early research by Bigham et al.,⁸ showing that it transforms over time to goethite. Following this initial discovery, a very large body of research has focused on understanding the transformation of schwertmannite to goethite and the consequences for the mobility and fate of co-associated elements. Indeed, the transformation of schwertmannite to goethite forms a fundamental and deep-rooted basis of our understanding on schwertmannite behavior and Fe cycling in acid-sulfate environments. This is evident by the fact that schwertmannite transformation to goethite has been mentioned in almost every published study involving schwertmannite since Bigham et al.'s publication⁸ almost 25 years ago. The field observations presented here may therefore be considered intriguing given that goethite was of negligible importance in the strongly acidic and As-rich AMD at the study site.

A previous study on schwertmannite-bearing acid sulfate soils has also reported a seeming absence of goethite, which was explained by stabilization of schwertmannite due to adsorbed Si, PO₄³⁻, and natural organic material (NOM).⁶³ This is somewhat consistent with laboratory-based experiments, showing that these species slow down or otherwise attenuate the extent of schwertmannite transformation to goethite.^{72–77} However, it disagrees with an abundance of field-based observations (where Si, PO₄³⁻, and NOM are ubiquitous), which show that schwertmannite typically occurs as mixtures with goethite.^{6,25,40,51,52,54,58} It also contradicts studies on sediment and terrace profiles from acid-sulfate

systems, where younger near-surface layers are schwertmannite-rich, while older subsurface layers contain increasing amounts of goethite.^{14,15,25,55,57,58}

Although goethite can retain appreciable amounts of As(V),⁴³ previous experimental work has consistently shown that adsorbed and coprecipitated As(V) retards the transformation of schwertmannite to goethite.^{16,24,26,30,32,78} For example, Regenspurg and Peiffer³⁰ found that coprecipitated As(V) retarded schwertmannite transformation to goethite at pH 4, by inhibiting the crystallization of goethite and simultaneously slowing the dissolution of schwertmannite. The results of the mineral transformation experiment described here are consistent with this earlier work, in so much as goethite formation was only observed in the As(V)-free treatment. However, our experimental results conflict with the parallel expectation of lower levels of schwertmannite transformation at higher As(V) levels. Interestingly, the results show that, contrary to inhibiting schwertmannite transformation, increasing levels of As(V) incorporation within schwertmannite significantly enhanced its transformation. However, the key point of distinction concerning this enhanced schwertmannite transformation is that the resulting mineral was jarosite rather than goethite.

Jarosite. While the vast majority of research effort on the topic of schwertmannite transformation has focused on goethite as the transformation product, it is clear that jarosite can also form as a schwertmannite transformation product under some conditions.^{9,13,59,79–81} Indeed, in the AMD system examined in this study, jarosite occurred in all samples collected downstream of the adit entrance, consistent with its formation as a product of schwertmannite transformation. Jarosite was also the only mineral product which formed in the presence of As(V) via transformation of schwertmannite and AFA in the mineral transformation experiment. Jarosite formation can be considered to be partly a consequence of the strongly acidic nature of the AMD examined in the present study as previous studies have demonstrated that pH < 3 favors the formation of jarosite over goethite.^{7,59} For example, in a study of an acidic mine pit lake, Sánchez-España et al.⁵⁹ found that jarosite formation from precursor schwertmannite was increasingly favored when pH decreased below 2.5. It also reflects availability of an adequate supply of K⁺ and SO₄²⁻ that is required for jarosite formation (with K⁺ being supplied from K-bearing minerals, such as feldspars, and SO₄²⁻ from oxidation of sulfide minerals).^{79,80}

Jarosite is part of the alunite supergroup of minerals, which consists of about 40 mineral species having the general formula AB₃(TO₄)₂(OH)₆. Minerals within this supergroup are capable of extensive exchange in the A, B, and T sites where A can be occupied by cations such K⁺, Na⁺, H₃O⁺, NH₄⁺, Ag⁺, or Pb²⁺; B is occupied by Fe³⁺ or Al³⁺; and the TO₄ site by anions such as SO₄²⁻, PO₄³⁻, or AsO₄³⁻.^{82,83} Within this large group, the jarosite sub-group is characterized by B = Fe³⁺ and T = S, with jarosite *stricto sensu* having A = K⁺ and natrojarosite having A = Na⁺. Hydronium jarosite (where A = H₃O⁺) is relatively rare, although most jarosite group minerals appear to contain some H₃O⁺ in the A site,⁵⁹ as appeared to be the case for jarosite formed in the AMD system examined here. This can be considered as a consequence of the strongly acidic nature of the AMD described in this study combined with its relatively low concentrations of K⁺ (i.e., where the activity of H₃O⁺ greatly exceeded K⁺).

Although solid-phase As was mainly associated with poorly crystalline phases (AFA and schwertmannite), the results nevertheless show that jarosite was also an important host phase for As along the AMD flow-path examined in this study. Arsenic(V)-bearing jarosite has been observed previously in mine wastes and associated AMD systems.^{38,82} Several studies have shown that jarosite can accommodate As(V) within its crystal structure by substitution of AsO_4^{3-} for SO_4^{2-} .^{84–86} In the present study, the highest observed molar As/(As + S) ratio in jarosite equates to 22 mol % substitution of AsO_4^{3-} for SO_4^{2-} (based on extraction data for samples where scorodite was absent and jarosite was the only detectable crystalline As- and S-bearing phase) (Supporting Information, Figure S5b). This shows excellent agreement with the highest level of AsO_4^{3-} for SO_4^{2-} substitution within jarosite (21 mol %) in aged material from the mineral transformation experiment (Figure S5b). These results concur with earlier laboratory-based experimental studies showing an upper limit for the extent of AsO_4^{3-} for SO_4^{2-} substitution between 20 and 25 mol %.^{84–86}

Scorodite. Scorodite was a common but only very minor phase in Fe(III) precipitates collected from AMD at the study site. The presence of scorodite in the samples examined in this study is consistent with its frequently reported occurrence in As-rich mine wastes.¹⁷ It also agrees with the thermodynamic stability of scorodite, whereby at aqueous As(V) activities above $\sim 10^{-6}$ (i.e., above $\sim 75 \mu\text{g L}^{-1}$), AFA, schwertmannite, and jarosite are all metastable with regard to scorodite under the pH conditions in AMD at the study site (Figure 13c). These aqueous As(V) activities also make scorodite more thermodynamically favorable than goethite (Figure 13c). This helps to explain the absence of goethite (or possible presence as a trace component only) and the presence of scorodite in the As-rich AMD system described here.

In this case, scorodite appears to be the thermodynamically favored end-product resulting from transformation of AFA, schwertmannite, and eventually jarosite under strongly acidic As-rich AMD conditions (Figure 13c). Its presence as only a very minor phase in the AMD system examined here likely reflects scorodite's very slow kinetics of formation at low temperature coupled with As and Fe sequestration via the relatively rapid formation of As-rich jarosite.⁸⁷ This concurs with the mineral transformation experiment, which found no evidence for scorodite, despite extensive transformation of AFA/schwertmannite to jarosite.

Novel Effect of As(V) on Transformation of Schwertmannite to Jarosite. The results from the mineral transformation experiment show that the greatest levels of jarosite formation occurred at intermediate Fe/As ratios. In this experiment, jarosite formed via transformation of schwertmannite at low As(V) levels and via transformation of AFA at high As(V) levels. The field-based observations from the study site also reveal a similar relationship between jarosite abundance and the Fe/As ratio. In this regard, the greatest abundance of jarosite also occurred at intermediate Fe/As ratios, with schwertmannite being of increasing importance toward higher Fe/As ratios [i.e., relatively low As(V) levels] and AFA being important at lower Fe/As ratios [i.e., relatively high As(V) levels]. Overall, this general agreement between field- and laboratory-based results suggests that jarosite formation was optimized at intermediate levels of As(V) enrichment along the spectrum between precursor schwertmannite and AFA.

The results imply that increasing degrees of As(V)-incorporation within schwertmannite led to greater levels of schwertmannite transformation to jarosite [despite As(V) completely inhibiting schwertmannite transformation to goethite]. Jarosite differs from goethite in that it can accommodate large amounts of As(V) within its crystal lattice, whereas significant As(V) incorporation does not occur in goethite (since AsO_4^{3-} is structurally incompatible with goethite). Peak levels of jarosite formation at 2 days in the mineral transformation experiment appear to match the lowest molar Fe/As ratio (i.e., 8) for schwertmannite formation (Figure 11). Schwertmannite did not form below this threshold molar Fe/As ratio because higher levels of As(V)-enrichment led to preferential formation of AFA. This switch to AFA formation under As(V)-rich conditions resulted in progressively lower levels of jarosite formation as As(V) increased. This accords with the greater thermodynamic stability of AFA over jarosite at relatively high As(V) concentrations, as shown in Figure 13b [i.e., abundant As(V) favors the persistence of AFA].

Under low to moderate As(V) concentrations and strongly acidic pH (and given sufficient K^+), schwertmannite is metastable with regard to jarosite (e.g., compare Figure 13a,b). Hence, under these conditions, the formation of jarosite is a function of the kinetics of schwertmannite transformation to jarosite. As such, the novel effect of As(V) in enhancing schwertmannite transformation to jarosite may be a result of accelerated dissolution rates for As(V)-rich schwertmannite. However, previous research by Regenspurg and Peiffer³⁰ suggests that increasing levels of As(V) incorporation within schwertmannite decreases its dissolution over time. From this earlier work, we would therefore expect that As(V) should impede the transformation of schwertmannite to jarosite—an expectation that contradicts our experimental results. Nevertheless, a critical point in considering the results of Regenspurg and Peiffer³⁰ is that their finding was derived from schwertmannite dissolution experiments in which neither goethite nor jarosite formed [due to As(V) poisoning goethite crystallization, and an absence of K^+ preventing jarosite formation]. This lack of jarosite formation (despite suitable pH) accords, more broadly, with the generally ubiquitous absence of K^+ in previous experimental examinations of schwertmannite stability under acidic conditions.^{8,16,26,30,32,50,58,72}

Clearly, aging of schwertmannite in the presence of an adequate amount of K^+ under strongly acidic (pH < 3) conditions enabled relatively rapid jarosite formation, regardless of the presence of As(V) (Figure 10). The apparent discrepancy with Regenspurg and Peiffer's³⁰ dissolution experiment can be reconciled by considering that Cruz-Hernández et al.¹⁶ recently found that As(V) coprecipitation decreases the crystallite size of schwertmannite (and possibly increases the level of disorder). These As(V)-induced decreases in crystalline size (and decreases in order) can translate to potential increases in schwertmannite dissolution rates. This potential increase will only be manifested in situations where the dissolution products of As(V)-bearing schwertmannite (Fe^{3+} , SO_4^{2-} , and AsO_4^{3-}) are continuously removed from solution; a situation that would occur via precipitation of As(V)-bearing jarosite (facilitated by the presence of K^+). Hence, it appears plausible that the effect of As(V) in accelerating schwertmannite transformation to jarosite may be related to enhanced schwertmannite

dissolution caused by increasing levels of As(V) incorporation and driven by simultaneous ongoing removal of aqueous Fe^{3+} , SO_4^{2-} , and AsO_4^{3-} by jarosite formation.

The finding that schwertmannite transformation to jarosite is accelerated by increasing levels of As(V)-incorporation within the initial schwertmannite raises the question: Why, then, does As(V)-rich schwertmannite appear to persist at the study site? To answer this question, it is important to recall that transformation of schwertmannite to jarosite requires an adequate supply of K^+ .^{79,80} Hence, the relatively low concentrations of K^+ in the AMD system described here very likely limit complete in situ schwertmannite transformation to jarosite, thereby enabling schwertmannite persistence. In addition to low K^+ concentrations, schwertmannite may be further stabilized by relatively high concentrations of Si, NOM, and other components, which are also present in the ochreous material at the study site. It should also be noted that the presence of schwertmannite in a field setting does not necessarily reflect its long-term persistence or stability. It may instead reflect dynamic ongoing formation processes that are related to, for example, active redox cycling of Fe (which is certainly fueling ongoing schwertmannite formation at various locations along the AMD flow-path at the study site).

CONCLUSIONS

This study provides new information for improved understanding of Fe(III) mineral behavior and related changes in As speciation and mobility in AMD systems. The results show that formation of Fe(III) minerals has played a key role in aqueous As attenuation in the AMD system examined here. This occurred primarily via structural incorporation of As(V) within AFA, schwertmannite and jarosite, leading to very high solid-phase As concentrations (up to ~20% w/w). Our results also provide field-based evidence highlighting the important impact that the development of reducing conditions in an AMD flow-path can have in remobilizing solid-phase As, via reductive dissolution of As(V)-bearing Fe(III) minerals and reduction of As(V) to As(III).

Our field and laboratory results show that in strongly acidic and As-rich AMD, the relative abundance of As(V) controls the initial formation of AFA versus schwertmannite, with particularly As-rich conditions favoring AFA formation. The results reveal that As(V) also has a prominent impact on the mineralogy of crystalline Fe(III) phases that are formed via transformation of poorly ordered precursor phases (such as AFA and schwertmannite). It is clear from the present study that highly elevated As concentrations in AMD systems can inhibit or otherwise prevent the formation of goethite. This is significant because the transformation of schwertmannite to goethite is a keystone concept in the environmental mineralogy of acid-sulfate systems. However, in strongly acidic and As-rich AMD, this mineralogical transformation pathway may be of negligible importance due to As-imposed shifts in Fe(III) mineral formation and stability.

This study has identified an important and previously unrecognized role that As(V) plays with regard to jarosite formation. The results show that increasing levels of As(V) incorporation in schwertmannite enhance its subsequent transformation to jarosite. This significant discovery necessitates a re-evaluation of the prevailing paradigm that As(V) simply retards schwertmannite transformation. It also emphasizes a general need for a more nuanced consideration of As(V)-rich jarosite formation in studies on schwertmannite

stability in AMD systems (with particular consideration of the presence of sufficient K). Future research is required to quantify the kinetics and mechanisms of this new As(V)-imposed effect on transformation of schwertmannite to jarosite.

ASSOCIATED CONTENT

Supporting Information

The Supporting Information is available free of charge at <https://pubs.acs.org/doi/10.1021/acsearthspacechem.1c00047>.

Study site, selected properties of Fe(III)-rich precipitates (identified according to their designated sample codes) formed from AMD at the study site, results for solid- and aqueous-phase composition of material produced from the mineral formation and transformation experiment, comparison of total As concentrations and oxalate-extractable (4 h at 80 °C) As concentrations in solid-phase samples collected from the study site, photographs of ochreous precipitates formed along the AMD flow-path at the study site, pH–Eh diagram showing stability fields for Fe species and aqueous-phase As species in comparison to pH–Eh conditions in pore-water and surface-water samples from the sediment retention pond, XRD patterns for solid-phase material produced in the mineral transformation experiment as a result of aging of the initial material for 2 and 5 days, and histograms of molar As/(As + S) ratios within poorly ordered and crystalline solid-phases occurring in AMD at the study site (PDF)

AUTHOR INFORMATION

Corresponding Author

Edward D. Burton – Southern Cross GeoScience, Southern Cross University, Lismore, New South Wales 2480, Australia; orcid.org/0000-0002-9628-089X; Email: ed.burton@scu.edu.au

Authors

Niloofer Karimian – Southern Cross GeoScience, Southern Cross University, Lismore, New South Wales 2480, Australia; orcid.org/0000-0002-8444-6610

Scott G. Johnston – Southern Cross GeoScience, Southern Cross University, Lismore, New South Wales 2480, Australia; orcid.org/0000-0002-5826-5613

Valerie A. Schoepfer – Department of Geological Sciences, University of Saskatchewan, Saskatoon, Saskatchewan S7N 5E2, Canada; orcid.org/0000-0002-9582-9940

Girish Choppala – College of Engineering, Science, and Environment, University of Newcastle, Callaghan, New South Wales 2308, Australia; orcid.org/0000-0002-8866-5001

Dane Lamb – College of Engineering, Science, and Environment, University of Newcastle, Callaghan, New South Wales 2308, Australia; orcid.org/0000-0003-2303-5460

Complete contact information is available at:

<https://pubs.acs.org/doi/10.1021/acsearthspacechem.1c00047>

Funding

This research was funded by a grant from the Australian Research Council (FT200100449). Use of the XAS Beamline at the Australian Synchrotron was supported by a grant from

the Australian Nuclear Science and Technology Organisation (AS211/XAS/16852).

Notes

The authors declare no competing financial interest.

ACKNOWLEDGMENTS

Analytical support was provided by the Environmental Analysis Laboratory (EAL), which is a Southern Cross University NATA-accredited research support facility. Laboratory assistance was provided by the Roz Hagan and Nicholas Ward. Technical assistance at the XAS beamline of the Australian Synchrotron was provided by Jessica Hamilton. We thank Andrew Sampaklis (Legacy Mines Program, NSW State Government) for providing information about the Ottery Mine site. We also thank Maxine Dawes for technical support with electron microscopy.

REFERENCES

- (1) Hudson-Edwards, K. Tackling mine wastes. *Science* **2016**, *352*, 288–290.
- (2) Nordstrom, D. K.; Blowes, D. W.; Ptacek, C. J. Hydrogeochemistry and microbiology of mine drainage: An update. *Appl. Geochem.* **2015**, *57*, 3–16.
- (3) Majzlan, J.; Drahota, P.; Filippi, M. Parageneses & crystal chemistry of As minerals. *Rev. Mineral. Geochem.* **2014**, *79*, 17–184.
- (4) Fukushi, K.; Sasaki, M.; Sato, T.; Yanase, N.; Amano, H.; Ikeda, H. A natural attenuation of arsenic in drainage from an abandoned arsenic mine dump. *Appl. Geochem.* **2003**, *18*, 1267–1278.
- (5) Asta, M. P.; Ayora, C.; Román-Ross, G.; Cama, J.; Acero, P.; Gault, A. G.; Charnock, J. M.; Bardelli, F. Natural attenuation of arsenic in the Tinto Santa Rosa acid stream (Iberian Pyritic Belt, SW Spain): the role of iron precipitates. *Chem. Geol.* **2010**, *271*, 1–12.
- (6) Abramov, S. M.; Tejada, J.; Grimm, L.; Schädler, F.; Bulaev, A.; Tomaszewski, E. J.; Byrne, J. M.; Straub, D.; Thorwarth, H.; Amils, R.; Kleindienst, S.; Kappler, A. Role of biogenic Fe(III) minerals as a sink and carrier of heavy metals in the Rio Tinto, Spain. *Sci. Total Environ.* **2020**, *718*, 137294.
- (7) Bigham, J. M.; Schwertmann, U.; Pfab, G. Influence of pH on mineral speciation in a bioreactor simulating acid mine drainage. *Appl. Geochem.* **1996**, *11*, 845–849.
- (8) Bigham, J. M.; Schwertmann, U.; Traina, S. J.; Winland, R. L.; Wolf, M. Schwertmannite and the chemical modeling of iron in acid sulfate waters. *Geochim. Cosmochim. Acta* **1996**, *60*, 2111–2121.
- (9) Egal, M.; Casiot, C.; Morin, G.; Parmentier, M.; Bruneel, O.; Lebrun, S.; Elbaz-Poulichet, F. Kinetic control on the formation of tooeleite, schwertmannite and jarosite by *Acidithiobacillus ferrooxidans* strains in an As(III)-rich acid mine water. *Chem. Geol.* **2009**, *265*, 432–441.
- (10) Rancourt, D. G.; Fortin, D.; Pichler, T.; Thibault, P.-J.; Lamarche, G.; Morris, R. V.; Mercier, P. H. J. Mineralogy of a natural As-rich hydrous ferric oxide coprecipitate formed by mixing of hydrothermal fluid and seawater: Implications regarding surface complexation and color banding in ferrihydrite deposits. *Am. Mineral.* **2001**, *86*, 834–851.
- (11) Carlson, L.; Bigham, J. M.; Schwertmann, U.; Kyek, A.; Wagner, F. Scavenging of As from acid mine drainage by schwertmannite and ferrihydrite: a comparison with synthetic analogues. *Environ. Sci. Technol.* **2002**, *36*, 1712–1719.
- (12) Maillot, F.; Morin, G.; Juillot, F.; Bruneel, O.; Casiot, C.; Ona-Nguema, G.; Wang, Y.; Lebrun, S.; Aubry, E.; Vlaic, G.; Brown, G. E. Structure and reactivity of As(III)- and As(V)-rich schwertmannites and amorphous ferric arsenate sulfate from the Carnoules acid mine drainage, France: Comparison with biotic and abiotic model compounds and implications for As remediation. *Geochim. Cosmochim. Acta* **2013**, *104*, 310–329.
- (13) Acero, P.; Ayora, C.; Torrentó, C.; Nieto, J.-M. The behaviour of trace elements during schwertmannite precipitation and subsequent transformation into goethite and jarosite. *Geochim. Cosmochim. Acta* **2006**, *70*, 4130–4139.
- (14) Parviainen, A.; Cruz-Hernández, P.; Pérez-López, R.; Nieto, J. M.; Delgado-López, J. M. Raman identification of Fe precipitates and evaluation of As fate during phase transformation in Tinto and Odiel River Basins. *Chem. Geol.* **2015**, *398*, 22–31.
- (15) Cruz-Hernández, P.; Pérez-López, R.; Parviainen, A.; Lindsay, M. B. J.; Nieto, J. M. Trace element-mineral associations in modern and ancient iron terraces in acid drainage environments. *Catena* **2016**, *147*, 386–393.
- (16) Cruz-Hernández, P.; Carrero, S.; Pérez-López, R.; Fernandez-Martinez, A.; Lindsay, M. B. J.; Dejoie, C.; Nieto, J. M. Influence of As(V) on precipitation and transformation of schwertmannite in acid mine drainage-impacted waters. *Eur. J. Mineral.* **2019**, *31*, 237–245.
- (17) Drahota, P.; Filippi, M. Secondary arsenic minerals in the environment: a review. *Environ. Int.* **2009**, *35*, 1243–1255.
- (18) Burton, E. D.; Bush, R. T.; Sullivan, L. A.; Johnston, S. G.; Hocking, R. K. Mobility of arsenic and selected metals during re-flooding of iron- and organic-rich acid-sulfate soil. *Chem. Geol.* **2008**, *253*, 64–73.
- (19) Arsic, M.; Teasdale, P. R.; Welsh, D. T.; Johnston, S. G.; Burton, E. D.; Hockmann, K.; Bennett, W. W. Diffusive gradients in thin films (DGT) reveals antimony and arsenic mobility differs in a contaminated wetland sediment during an oxic-anoxic transition. *Environ. Sci. Technol.* **2018**, *52*, 1118–1127.
- (20) Karimian, N.; Johnston, S. G.; Burton, E. D. Iron and sulfur cycling in acid sulfate soil wetlands under dynamic redox conditions: a review. *Chemosphere* **2018**, *197*, 803–816.
- (21) Johnston, S. G.; Karimian, N.; Burton, E. D. Seasonal temperature oscillations drive contrasting arsenic and antimony mobilisation in a mining-impacted river system. *Water Resour. Res.* **2020**, *56*, No. e2020WR028196.
- (22) Tabelin, C. B.; Corpuz, R. D.; Igarashi, T.; Villacorte-Tabelin, M.; Alorro, R. D.; Yoo, K.; Raval, S.; Ito, M.; Hiroyoshi, N. Acid mine drainage formation and arsenic mobility under strongly acidic conditions: Importance of soluble phases, iron oxyhydroxides/oxides and nature of oxidation layer on pyrite. *J. Hazard. Mater.* **2020**, *399*, 122844.
- (23) Kumpulainen, S.; Räisänen, M.-L.; von der Kammer, F.; Hofmann, T. Ageing of synthetic and natural schwertmannites at pH 2–8. *Clay Miner.* **2008**, *43*, 437–448.
- (24) Burton, E. D.; Johnston, S. G.; Watling, K.; Bush, R. T.; Keene, A. F.; Sullivan, L. A. Arsenic effects and behaviour in association with the Fe(II)-catalysed transformation of schwertmannite. *Environ. Sci. Technol.* **2010**, *44*, 2016.
- (25) Park, J. H.; Han, Y.-S.; Ahn, J. S. Comparison of arsenic coprecipitation and adsorption by iron minerals and the mechanism of arsenic natural attenuation in a mine stream. *Water Res.* **2016**, *106*, 295–303.
- (26) Cruz-Hernández, P.; Pérez-López, R.; Nieto, J. M. Role of arsenic during the aging of acid mine drainage precipitates. *Procedia Earth Planet. Sci.* **2017**, *17*, 233–236.
- (27) Kim, H.-J.; Kim, Y. Schwertmannite transformation to goethite and the related mobility of trace metals in acid mine drainage. *Chemosphere* **2021**, *269*, 128720.
- (28) Burton, E. D.; Bush, R. T.; Sullivan, L. A.; Mitchell, D. R. G. Schwertmannite transformation to goethite via the Fe(II) pathway: reaction rates and implications for iron-sulfide formation. *Geochim. Cosmochim. Acta* **2008**, *72*, 4551–4564.
- (29) McCleskey, R. B.; Nordstrom, D. K.; Maest, A. S. Preservation of water samples for arsenic(III/V) determinations: an evaluation of the literature and new analytical results. *Appl. Geochem.* **2004**, *19*, 995–1009.
- (30) Regenspurg, S.; Peiffer, S. Arsenate and chromate incorporation in schwertmannite. *Appl. Geochem.* **2005**, *20*, 1226–1239.
- (31) Antelo, J.; Fiol, S.; Gondar, D.; Pérez, C.; López, R.; Arce, F. Cu(II) incorporation to schwertmannite: Effect on stability and reactivity under AMD conditions. *Geochim. Cosmochim. Acta* **2013**, *119*, 149–163.

- (32) Wang, Y.; Gao, M.; Huang, W.; Wang, T.; Liu, Y. Effects of extreme pH conditions on the stability of As(V)-bearing schwertmannite. *Chemosphere* **2020**, *251*, 126427.
- (33) Wu, D.; Sun, S. Speciation analysis of As, Sb and Se. *Trends Environ. Anal. Chem.* **2016**, *11*, 9–22.
- (34) Fadrus, H.; Malý, J. Suppression of iron(III) interference in determination of iron(II) in water by 1,10 phenanthroline method. *Analyst* **1975**, *100*, 549–554.
- (35) Schwertmann, U.; Cornell, R. M. *Iron Oxides in the Laboratory: Preparation and Characterization*; Wiley-VCH: NY, 2000.
- (36) Mikutta, C.; Mandaliev, P. N.; Kretzschmar, R. New clues to the local atomic structure of short-range ordered ferric arsenate from extended X-ray absorption fine structure spectroscopy. *Environ. Sci. Technol.* **2013**, *47*, 3122–3131.
- (37) Drahotová, P.; Grösslová, Z.; Kindlová, H. Selectivity assessment of an arsenic sequential extraction procedure for evaluating mobility in mine wastes. *Anal. Chim. Acta* **2014**, *839*, 34–43.
- (38) Hudson-Edwards, K. A. Uptake and release of arsenic and antimony in alunite-jarosite and beudantite group minerals. *Am. Mineral.* **2019**, *104*, 633–640.
- (39) Basciano, L. C.; Peterson, R. C. Jarosite-hydronium jarosite solid-solution series with full iron site occupancy: Mineralogy and crystal chemistry. *Am. Mineral.* **2007**, *92*, 1464–1473.
- (40) Johnston, S. G.; Keene, A. F.; Burton, E. D.; Bush, R. T.; Sullivan, L. A.; McElnea, A. E.; Ahern, C. R.; Smith, C. D.; Powell, B. Arsenic mobilisation in a seawater inundated acid sulfate soil. *Environ. Sci. Technol.* **2010**, *44*, 1968.
- (41) Blanc, P.; Lassin, A.; Piantone, P.; Azaroual, M.; Jacquemet, N.; Fabbri, A.; Gaucher, E. C. Thermoddb: a geochemical database focused on low temperature water/rock interactions and waste materials. *Appl. Geochem.* **2012**, *27*, 2107–2116.
- (42) Inskeep, W. P.; Maccur, R. E.; Harrison, G.; Bostick, B. C.; Fendorf, S. Biomineralization of As(V)-hydrous ferric oxyhydroxide in microbial mats of an acid-sulfate-chloride geothermal spring, Yellowstone National Park. *Geochim. Cosmochim. Acta* **2004**, *68*, 3141–3155.
- (43) Asta, M. P.; Cama, J.; Martínez, M.; Giménez, J. Arsenic removal by goethite and jarosite in acidic conditions and its environmental implications. *J. Hazard. Mater.* **2009**, *171*, 965–972.
- (44) Paktunc, D.; Dutrizac, J.; Gertsman, V. Synthesis and phase transformations involving scorodite, ferric arsenate and arsenical ferrihydrite: implications for arsenic mobility. *Geochim. Cosmochim. Acta* **2008**, *72*, 2649–2672.
- (45) Drahotová, P.; Knappová, M.; Kindlová, H.; Culka, A.; Majzlan, J.; Mihaljevič, M.; Rohovec, J.; Veselovský, F.; Fridrichová, M.; Jehlička, J. Mobility and attenuation of arsenic in sulfide-rich mining wastes from the Czech Republic. *Sci. Total Environ.* **2016**, *557*–558, 192–203.
- (46) Jelenová, H.; Majzlan, J.; Amoako, F. Y.; Drahotová, P. Geochemical and mineralogical characterization of the arsenic-, iron-, and sulfur-rich mining waste dumps near Kaňk, Czech Republic. *Appl. Geochem.* **2018**, *97*, 247–255.
- (47) Filippi, M.; Drahotová, P.; Machovič, V.; Böhmová, V.; Mihaljevič, M. Arsenic mineralogy and mobility in the arsenic-rich historical mine waste dump. *Sci. Total Environ.* **2015**, *536*, 713–728.
- (48) Bigham, J. M.; Carlson, L.; Murad, E. Schwertmannite, a new iron oxyhydroxysulfate from Pyhäsalmi, Finland, and other localities. *Mineral. Mag.* **1994**, *58*, 641–648.
- (49) Bigham, J. M.; Nordstrom, D. K. Iron and aluminium hydroxysulfates from acid sulfate waters. In *Sulfate Minerals: Crystallography, Geochemistry and Environmental Significance*; Alpers, C. N., Jambor, J. L., Nordstrom, D. K., Eds.; Reviews in Mineralogy and Geochemistry; Mineralogical Society of America, 2000; Vol. 40, pp 351–403.
- (50) Jönsson, J.; Persson, P.; Sjöberg, S.; Lövgren, L. Schwertmannite precipitated from acid mine drainage: phase transformation, sulphate release and surface properties. *Appl. Geochem.* **2005**, *20*, 179–191.
- (51) Courtin-Nomade, A.; Grosbois, C.; Bril, H.; Roussel, C. Spatial variability of arsenic in some iron-rich deposits generated by acid mine drainage. *Appl. Geochem.* **2005**, *20*, 383–396.
- (52) Bigham, J. M.; Schwertmann, U.; Carlson, L.; Murad, E. A poorly crystallized oxyhydroxysulfate of iron formed by bacterial oxidation of Fe(II) in acid mine waters. *Geochim. Cosmochim. Acta* **1990**, *54*, 2743–2758.
- (53) Peretyazhko, T.; Zachara, J. M.; Boily, J.-F.; Xia, Y.; Gassman, P. L.; Arey, B. W.; Burgos, W. D. Mineralogical transformations controlling acid mine drainage chemistry. *Chem. Geol.* **2009**, *262*, 169–178.
- (54) Yu, J.-Y.; Heo, B.; Choi, I.-K.; Cho, J.-P.; Chang, H.-W. Apparent solubilities of schwertmannite and ferrihydrite in natural stream waters polluted by mine drainage. *Geochim. Cosmochim. Acta* **1999**, *63*, 3407–3416.
- (55) Gagliano, W. B.; Brill, M. R.; Bigham, J. M.; Jones, F. S.; Traina, S. J. Chemistry and mineralogy of ochreous sediments in a constructed mine drainage wetland. *Geochim. Cosmochim. Acta* **2004**, *68*, 2119–2128.
- (56) Burgos, W. D.; Borch, T.; Troyer, L. D.; Luan, F.; Larson, L. N.; Brown, J. F.; Lambson, J.; Shimizu, M. Schwertmannite and Fe oxides formed by biological low-pH Fe(II) oxidation versus abiotic neutralization: impact on trace metal sequestration. *Geochim. Cosmochim. Acta* **2012**, *76*, 29–44.
- (57) Peine, A.; Tritschler, A.; Küsel, K.; Peiffer, S. Electron flow in an iron-rich acidic sediment – evidence for an acidity-driven iron cycle. *Limnol. Oceanogr.* **2000**, *45*, 1077–1087.
- (58) Regenspurg, S.; Brand, A.; Peiffer, S. Formation and stability of schwertmannite in acidic mining lakes. *Geochim. Cosmochim. Acta* **2004**, *68*, 1185–1197.
- (59) Sánchez-España, J.; Yusta, I.; López, G. A. Schwertmannite to jarosite conversion in the water column of an acidic mine pit lake. *Mineral. Mag.* **2012**, *76*, 2659–2682.
- (60) Miot, J.; Lu, S.; Morin, G.; Adra, A.; Benzerara, K.; Küsel, K. Iron mineralogy across the oxycline of a lignite mine lake. *Chem. Geol.* **2016**, *434*, 28–42.
- (61) Burton, E. D.; Bush, R. T.; Sullivan, L. A. Sedimentary iron geochemistry in acidic waterways associated with coastal lowland acid sulfate soils. *Geochim. Cosmochim. Acta* **2006**, *70*, 5445–5468.
- (62) Burton, E. D.; Bush, R. T.; Sullivan, L. A.; Mitchell, D. R. G. Reductive transformation of iron and sulfur in schwertmannite-rich accumulations associated with acidified coastal lowlands. *Geochim. Cosmochim. Acta* **2007**, *71*, 4456–4473.
- (63) Collins, R. N.; Jones, A. M.; Waite, T. D. Schwertmannite stability in acidified coastal environments. *Geochim. Cosmochim. Acta* **2010**, *74*, 482–496.
- (64) Johnston, S. G.; Keene, A. F.; Bush, R. T.; Burton, E. D.; Sullivan, L. A.; Isaacson, L.; McElnea, A. E.; Ahern, C. R.; Smith, C. D.; Powell, B. Iron geochemical zonation in a tidally inundated acid sulfate soil wetland. *Chem. Geol.* **2011**, *280*, 257–270.
- (65) Fitzpatrick, R. W.; Mosley, L. M.; Raven, M. D.; Shand, P. Schwertmannite formation and properties in acidic drain environments following exposure and oxidation of acid sulfate soils in irrigation areas during extreme drought. *Geoderma* **2017**, *308*, 235–251.
- (66) French, R. A.; Caraballo, M. A.; Kim, B.; Rimstidt, J. D.; Murayama, M.; Hochella, M. F. The enigmatic iron oxyhydroxysulfate nanomineral schwertmannite: Morphology, structure, and composition. *Am. Mineral.* **2012**, *97*, 1469–1482.
- (67) Fernandez-Martinez, A.; Timon, V.; Roman-Ross, G.; Cuello, G. J.; Daniels, J. E.; Ayora, C. The structure of schwertmannite, a nanocrystalline iron oxyhydroxysulfate. *Am. Mineral.* **2010**, *95*, 1312–1322.
- (68) Caraballo, M. A.; Rimstidt, J. D.; Macías, F.; Nieto, J. M.; Hochella, M. F. Metastability, nanocrystallinity and pseudo-solid solution effects on the understanding of schwertmannite solubility. *Chem. Geol.* **2013**, *360*–361, 22–31.

(69) Waychunas, G. A.; Xu, N.; Fuller, N.; Davis, J. A.; Bigham, J. M. XAS study of AsO₄³⁻ and SeO₄²⁻ substituted schwertmannite. *Phys. B* **1995**, *208–209*, 481–483.

(70) Burton, E. D.; Bush, R. T.; Johnston, S. G.; Watling, K. M.; Hocking, R. K.; Sullivan, L. A.; Parker, G. K. Sorption of arsenic(V) and arsenic(III) to schwertmannite. *Environ. Sci. Technol.* **2009**, *43*, 9202–9207.

(71) Antelo, J.; Fiol, S.; Gondar, D.; López, R.; Arce, F. Comparison of arsenate, chromate and molybdate binding on schwertmannite: Surface adsorption vs anion-exchange. *J. Colloid Interface Sci.* **2012**, *386*, 338–343.

(72) Knorr, K.-H.; Blodau, C. Controls on schwertmannite transformation rates and products. *Appl. Geochem.* **2007**, *22*, 2006–2015.

(73) Jones, A. M.; Collins, R. N.; Rose, J.; Waite, T. D. The effect of silica and natural organic matter on the Fe(II)-catalysed transformation and reactivity of Fe(III) minerals. *Geochim. Cosmochim. Acta* **2009**, *73*, 4409–4422.

(74) Burton, E. D.; Johnston, S. G. Impact of silica on the reductive transformation of schwertmannite and the mobilization of arsenic. *Geochim. Cosmochim. Acta* **2012**, *96*, 134–153.

(75) Schoepfer, V. A.; Burton, E. D.; Johnston, S. G.; Kraal, P. Phosphate imposed constraints on schwertmannite stability under reducing conditions. *Environ. Sci. Technol.* **2017**, *51*, 9739–9746.

(76) Schoepfer, V. A.; Burton, E. D.; Johnston, S. G. Contrasting effects of phosphate on the rapid transformation of schwertmannite to Fe(III) (oxy)hydroxides at near-neutral pH. *Geoderma* **2019**, *340*, 115–123.

(77) Schoepfer, V. A.; Burton, E. D.; Johnston, S. G.; Kraal, P. Phosphate loading alters schwertmannite transformation rates and pathways during microbial reduction. *Sci. Total Environ.* **2019**, *657*, 770–780.

(78) Antelo, J.; Fiol, S.; Carabante, I.; Arroyo, A.; Lezama-Pacheco, J. S.; Josevska, N.; Protopapa, C.; Kumpiene, J. Stability of naturally occurring AMD–schwertmannite in the presence of arsenic and reducing agents. *J. Geochem. Explor.* **2021**, *220*, 106677.

(79) Wang, H.; Bigham, J. M.; Tuovinen, O. H. Formation of schwertmannite and its transformation to jarosite in the presence of acidophilic iron-oxidizing microorganisms. *Mater. Sci. Eng., C* **2006**, *26*, 588–592.

(80) Gramp, J. P.; Jones, F. S.; Bigham, J. M.; Tuovinen, O. H. Monovalent cation concentrations determine the types of Fe(III) hydroxysulfate precipitates formed in bioleach solutions. *Hydrometallurgy* **2008**, *94*, 29–33.

(81) Sánchez España, J.; Santofimia Pastor, E.; López Pamo, E. Iron terraces in acid mine drainage systems: A discussion about the organic and inorganic factors involved in their formation through observations from the Tintillo acidic river (Riotinto mine, Huelva, Spain). *Geosphere* **2007**, *3*, 133–151.

(82) Sánchez-España, J.; Yusta, I.; Gray, J.; Burgos, W. D. Geochemistry of dissolved aluminum at low pH: Extent and significance of Al–Fe(III) coprecipitation below pH 4.0. *Geochim. Cosmochim. Acta* **2016**, *175*, 128–149.

(83) Dutrizac, J. E.; Jambor, J. L. Jarosites and their application in hydrometallurgy. *Rev. Mineral. Geochem.* **2000**, *40*, 405–452.

(84) Paktunc, D. Characterization of arsenate-for-sulfate substitution in synthetic jarosite using X-ray diffraction and X-ray absorption spectroscopy. *Can. Mineral.* **2003**, *41*, 905–919.

(85) Savage, K. S.; Bird, D. K.; O'Day, P. A. Arsenic speciation in synthetic jarosite. *Chem. Geol.* **2005**, *215*, 473–498.

(86) Aguilar-Carrillo, J.; Villalobos, M.; Pi-Puig, T.; Escobar-Quiroz, I. N.; Romero, F. M. Synergistic arsenic(V) and lead(II) retention on synthetic jarosite. I. Simultaneous structural incorporation behaviour and mechanism. *Environ. Sci. Processes & Impacts* **2018**, *20*, 354–369.

(87) Le Berre, J. F.; Gauvin, R.; Demopoulos, G. P. A study of the crystallization kinetics of scorodite via the transformation of poorly crystalline ferric arsenate in weakly acidic solution. *Colloids Surf., A* **2008**, *315*, 117–129.